Od neuronu do sieci: modelowanie układu nerwowego

Wybrane aspekty modelowania układu wzrokowego

dr Daniel Wójcik

http://www.neuroinf.pl/Members/danek/private_folder/theoretical_neuroscience/workshop

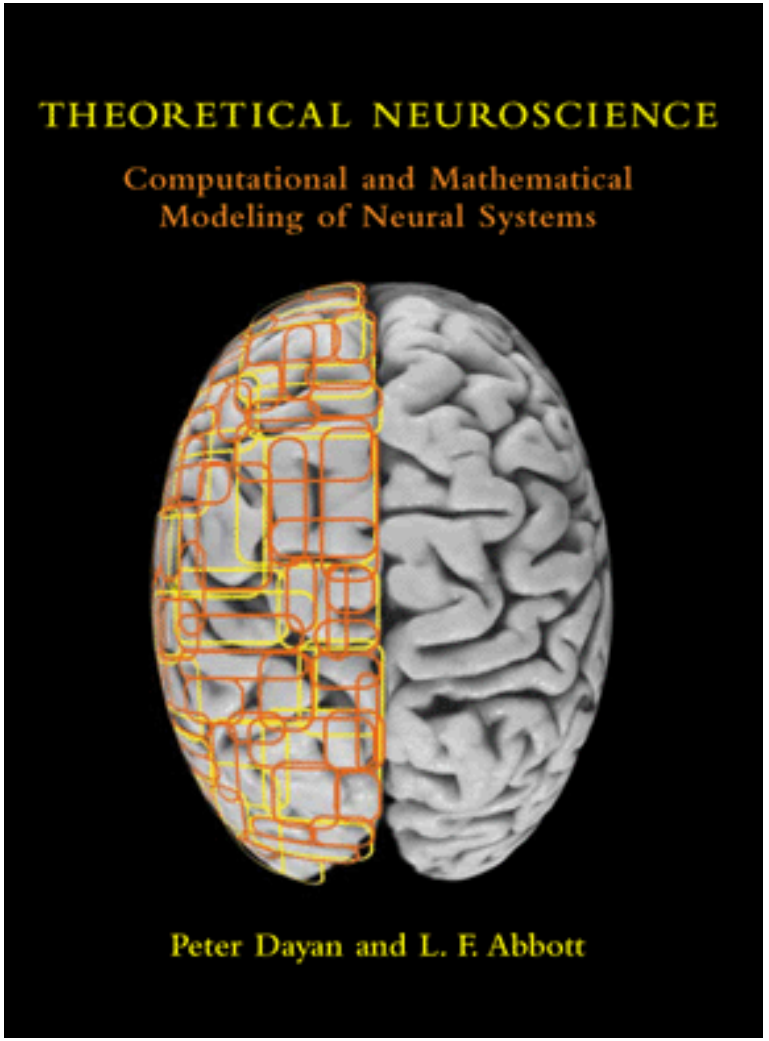

Na podstawie podręcznika

THEORETICAL NEUROSCIENCE

Petera Dayana i Larry'ego F. Abbotta

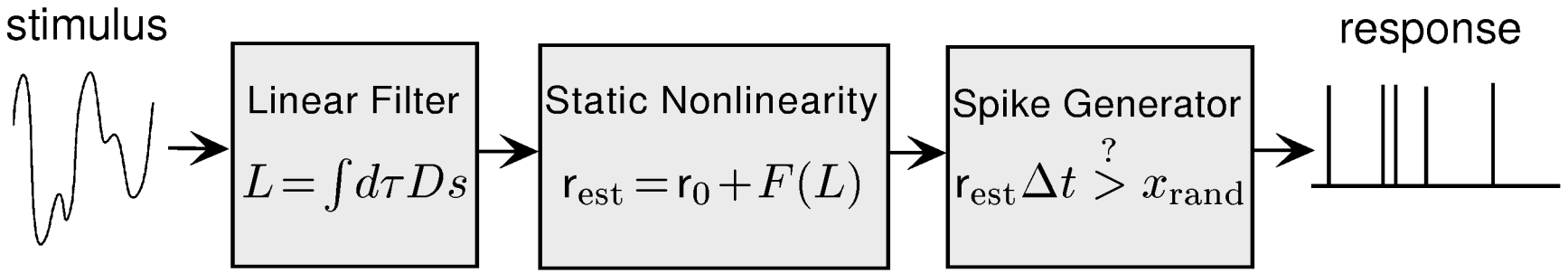

Figure 2.3 Simulating spiking responses to stimuli. The integral of the stimulus s times the optimal kernel D is first computed. The estimated firing rate is the background rate r_0 plus a nonlinear function of the output of the linear filter calculation. Finally, the estimated firing rate is used to drive a Poisson process that generates spikes.

A

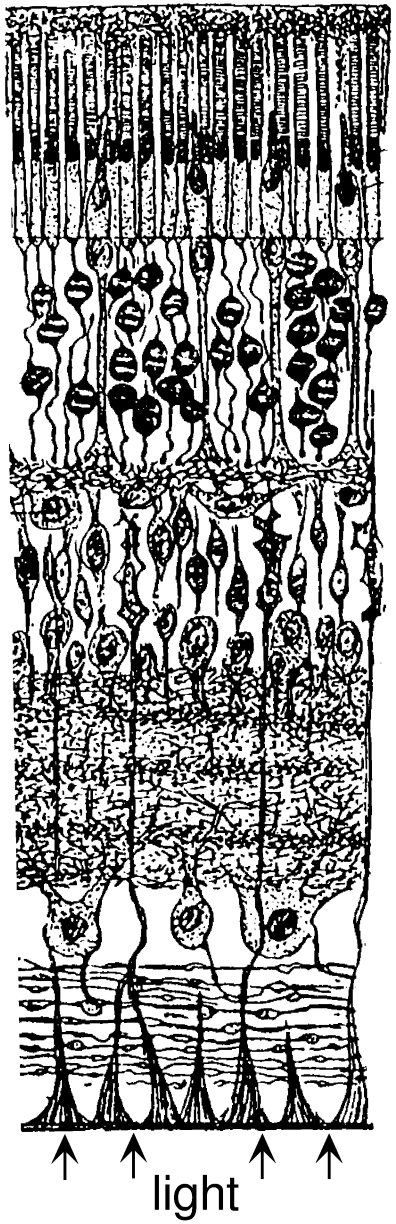

rod and cone receptors (R)

horizontal (H)

bipolar (B)

amacrine (A)

retinal ganglion (G)

B

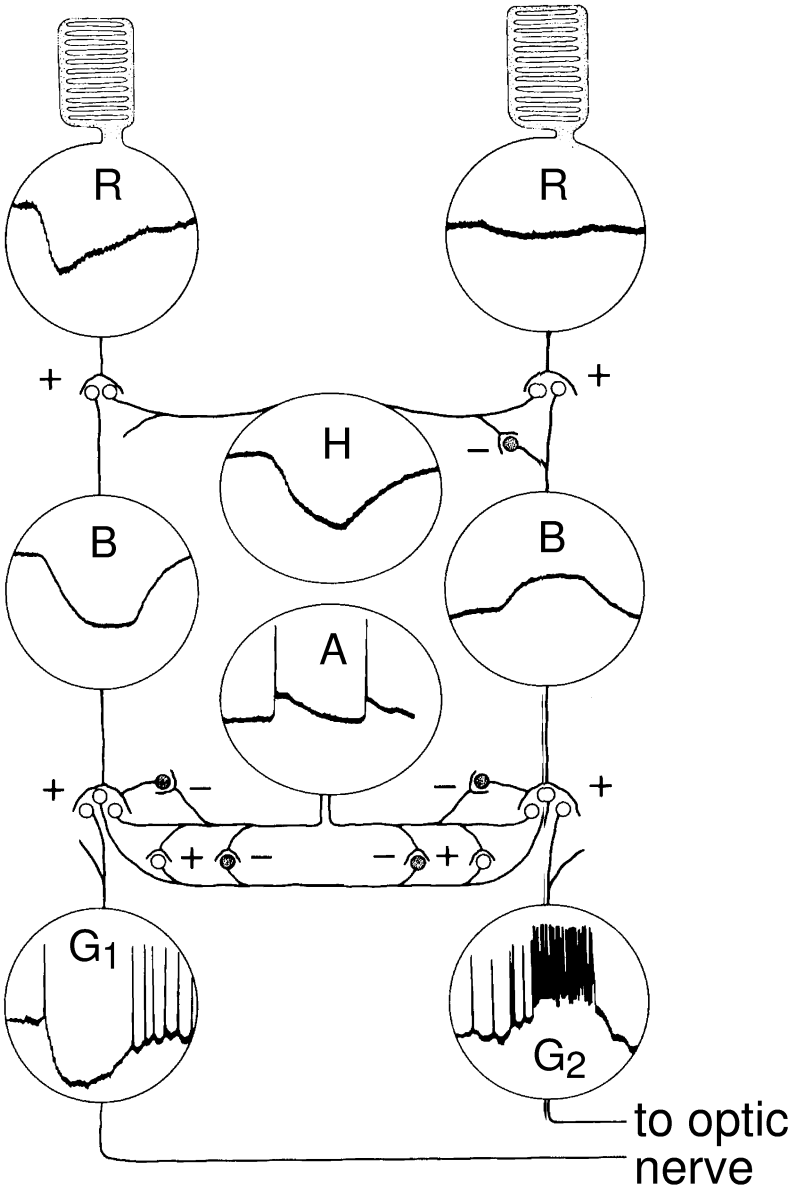

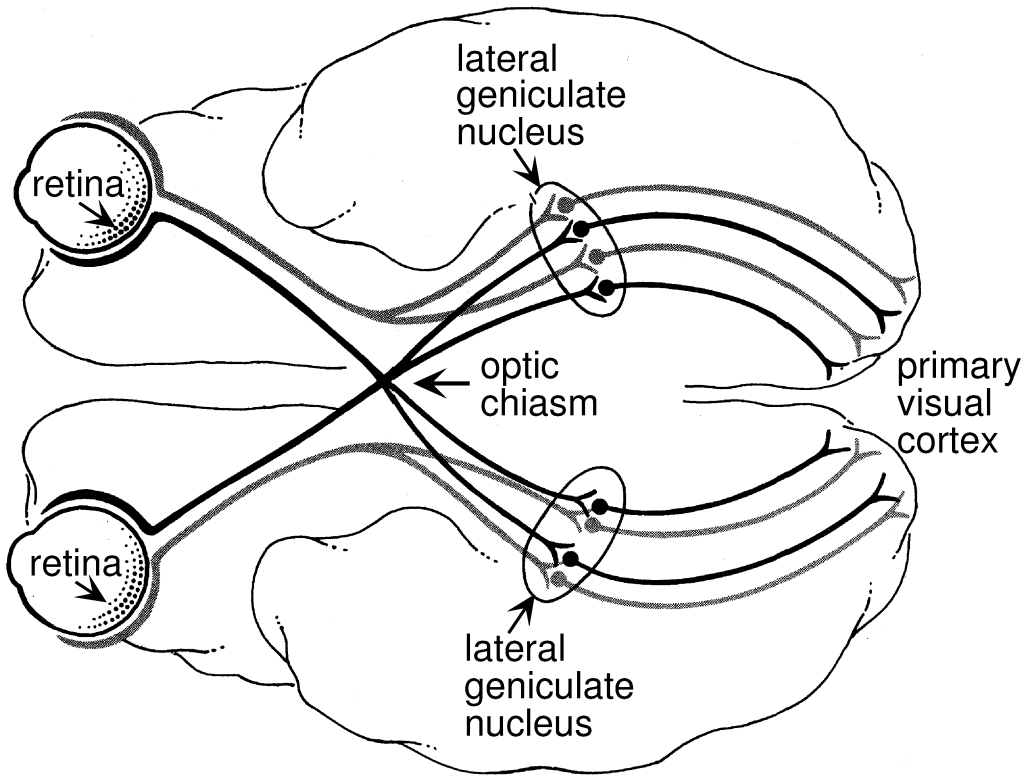
lateral
geniculate
nucleus
retina
optic
chiasm
primary
visual
cortex
retina
lateral
geniculate
nucleus

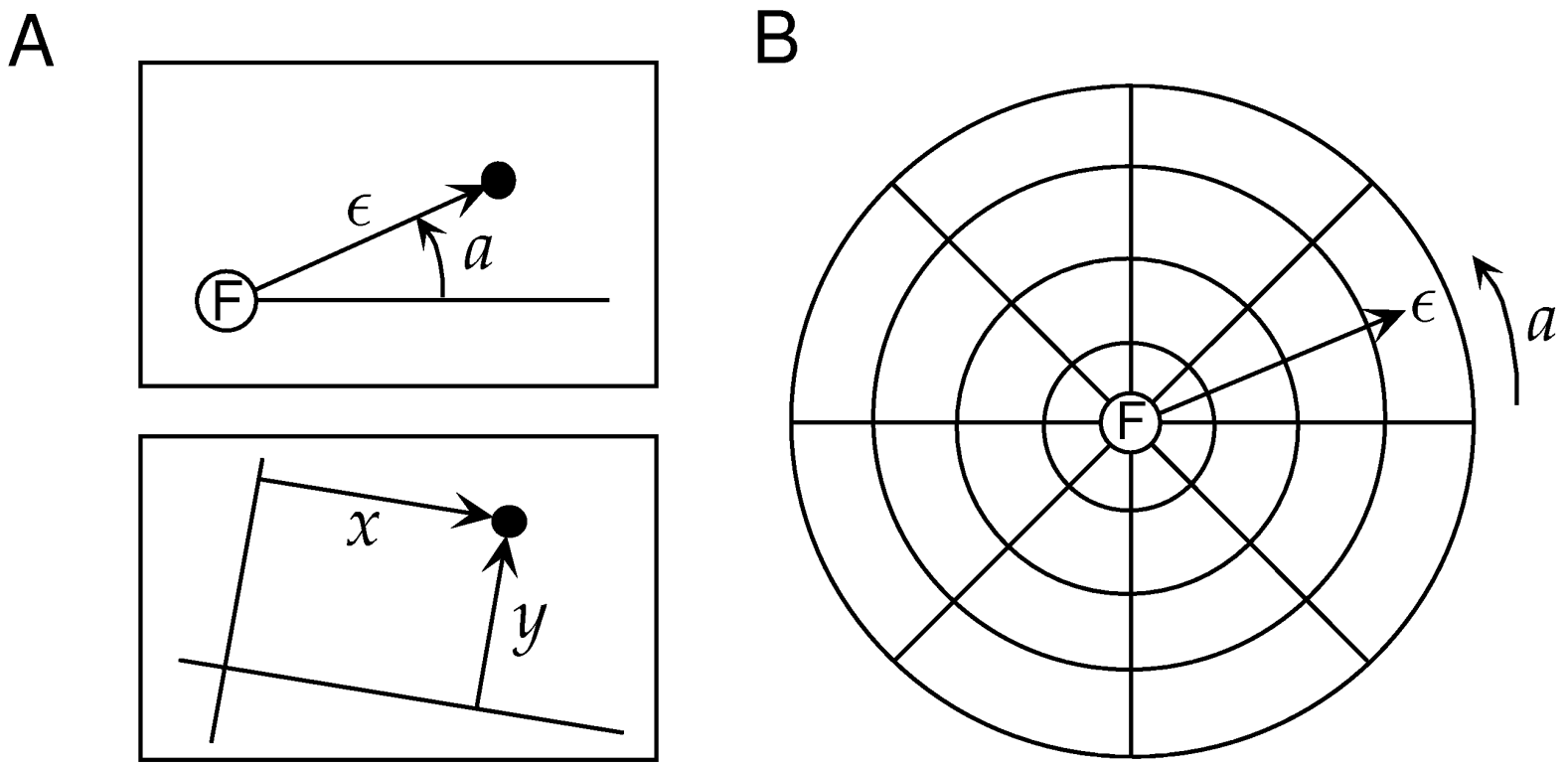
A
ϵ
a
F
x
y
B
ϵ
a
F

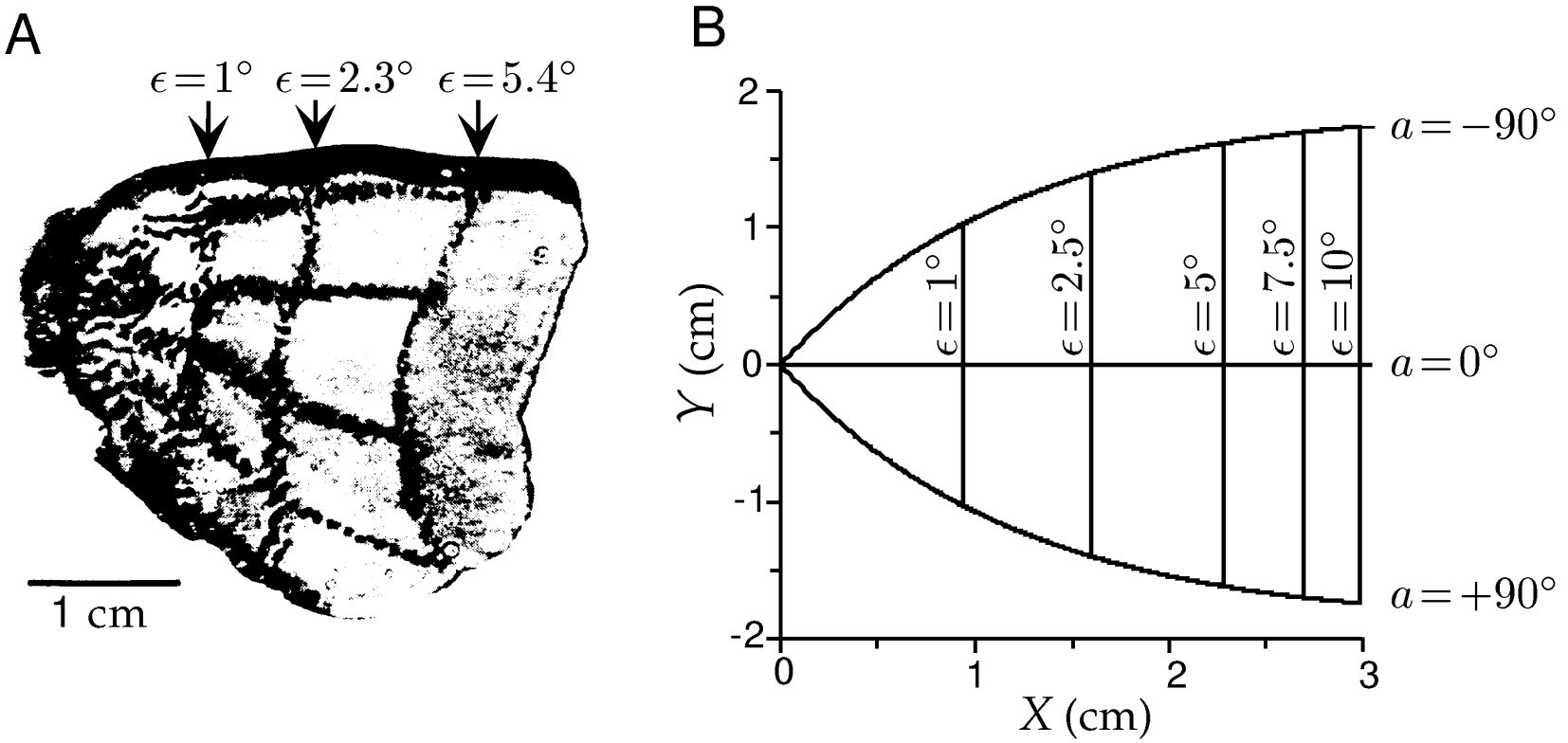
A
$\epsilon = 1°$ $\epsilon = 2.3°$ $\epsilon = 5.4°$
1 cm
B
$\epsilon = 1°$
$\epsilon = 2.5°$
$\epsilon = 5°$
$\epsilon = 7.5°$
$\epsilon = 10°$
$a = -90°$
$a = 0°$
$a = +90°$
Y (cm)
X (cm)
2
1
0
-1
-2
0
1
2
3

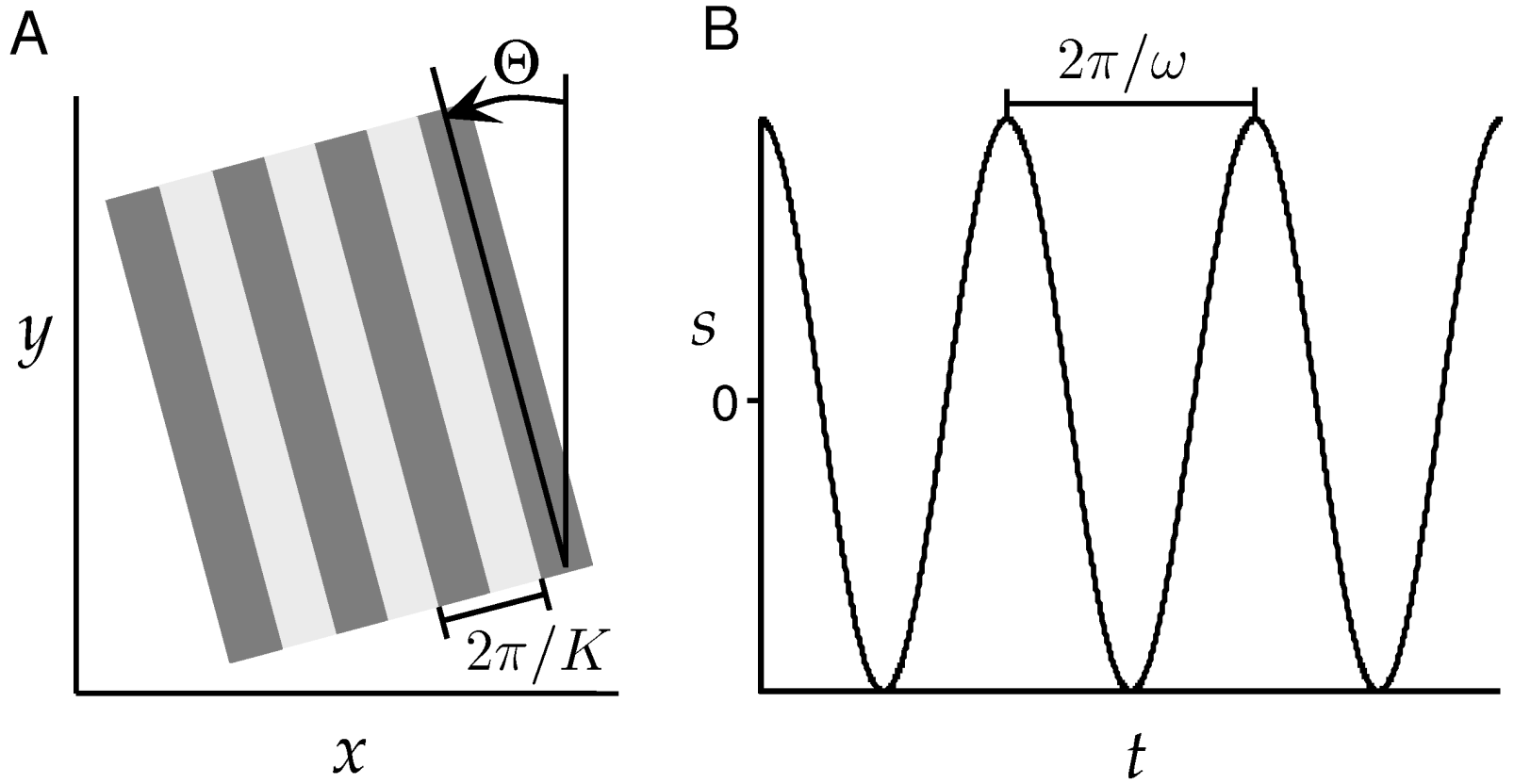
A
Θ
y
2π/K
x
B
2π/ω
s
0
t

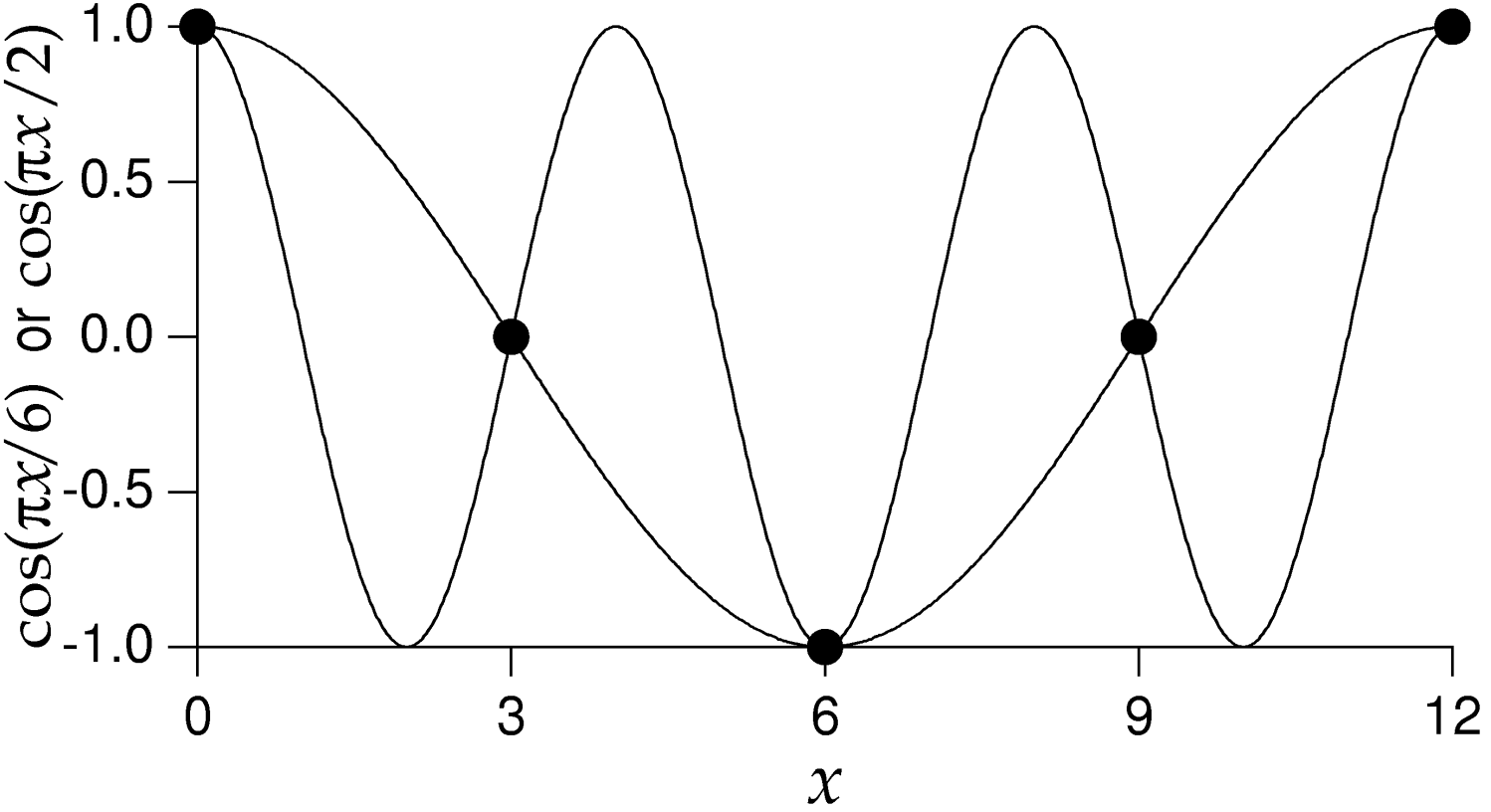
1.0
0.5
0.0
-0.5
-1.0
cos(πx/6) or cos(πx/2)
0
3
6
9
12
x

Metody korelacji odwrotnych: komórki proste

- Średni bodziec wyzwolony iglicą dla bodźców wzrokowych zależy od położenia i czasu

$$C(x, y, \tau) = \frac{1}{\langle n \rangle} \left\langle \sum_{i=1}^{n} s(x, y, t_i - \tau) \right\rangle$$

- Wiąże się z funkcją korelacji krzyżowej bodziec-częstość generacji iglic

$$Q_{rs}(x, y, \tau) = \frac{1}{T} \int_0^T dt\, r(t) s(x, y, t + \tau)$$

- wzorem

$$C(x, y, \tau) = \frac{Q_{rs}(x, y, -\tau)}{\langle r \rangle}$$

Liniowe oszacowanie częstości

- Będziemy szukać częstości generacji iglic w postaci $\mathrm{r}_{\mathrm{est}}(t) = \mathrm{r}_0 + F(L(t))$, gdzie

$$L(t) = \int_0^\infty d\tau \int dx dy \, D(x, y, \tau) s(x, y, t - \tau)$$

- Dla bodźca będącego białym szumem

$$D(x, y, \tau) = \frac{Q_{\mathrm{rs}}(x, y, -\tau)}{\sigma_s^2} = \frac{\langle r \rangle C(x, y, \tau)}{\sigma_s^2}$$

- Jądro $D(x, y, \tau)$ definiuje czasoprzestrzenne pole recepcyjne neuronu.

Pola recepcyjne

- Pole recepcyjne $D(x, y, \tau)$ niektórych neuronów można rozseparować

$$D(x, y, \tau) = D_{\mathrm{s}}(x, y) D_{\mathrm{t}}(\tau)$$

- Mówimy wtedy o separowalnym polu recepcyjnym. $D_{\mathrm{s}}(x, y)$ nazywamy wtedy przestrzennym polem recepcyjnym, $D_{\mathrm{t}}(\tau)$ czasowym polem recepcyjnym.

- Zwykle normalizujemy $D_{\mathrm{s}}(x, y)$ tak, żeby po całkowaniu dawało 1.

Przestrzenne pola recepcyjne

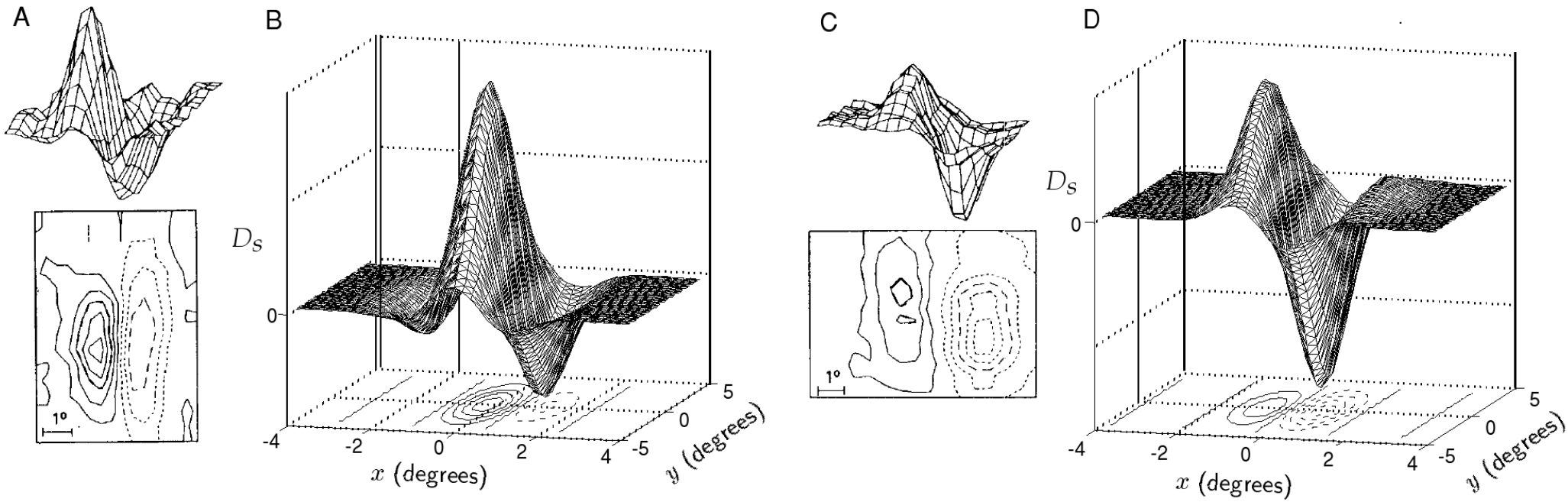

Figure 2.10 Spatial receptive field structure of simple cells. (A) and (C) Spatial structure of the receptive fields of two neurons in cat primary visual cortex determined by averaging stimuli between 50 ms and 100 ms prior to an action potential. The upper plots are three-dimensional representations, with the horizontal dimensions acting as the x-y plane and the vertical dimension indicating the magnitude and sign of $D_s(x, y)$. The lower contour plots represent the x-y plane. Regions with solid contour curves are ON areas where $D_s(x, y) > 0$, and regions with dashed contours are OFF areas where $D_s(x, y) < 0$. (B) and (D) Gabor functions (equation 2.27) with $\sigma_x = 1°$, $\sigma_y = 2°$, $1/k = 0.56°$, and $\phi = 1 - \pi/2$ (B) or $\phi = 1 - \pi$ (D), chosen to match the receptive fields in A and C. (A and C adapted from Jones and Palmer, 1987a.)

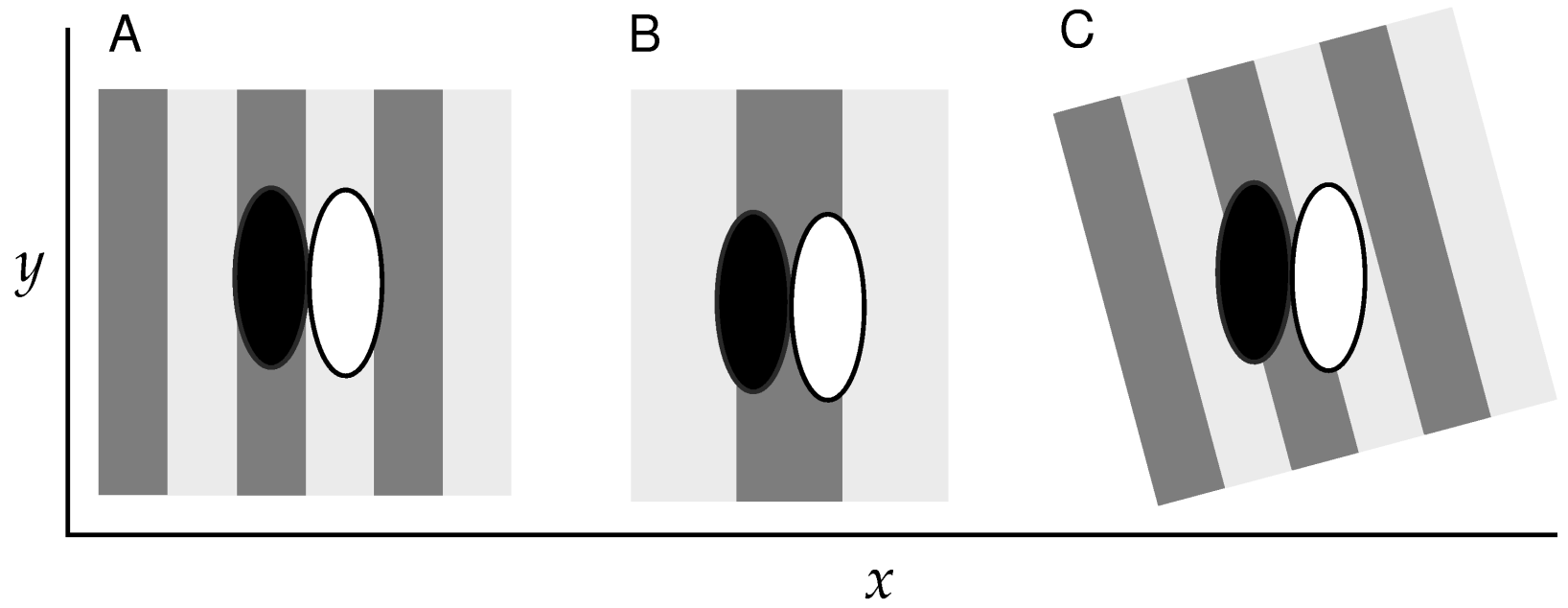

Figure 2.11 Grating stimuli superimposed on spatial receptive fields similar to those shown in figure 2.10. The receptive field is shown as two oval regions, one dark to represent an OFF area where $D_s < 0$ and one white to denote an ON region where $D_s > 0$. (A) A grating with the spatial wavelength, orientation, and spatial phase shown produces a high firing rate because a dark band completely overlaps the OFF area of the receptive field and a light band overlaps the ON area. (B) The grating shown is nonoptimal due to a mismatch in both the spatial phase and frequency, so that the ON and OFF regions each overlap both light and dark stripes. (C) The grating shown is at a nonoptimal orientation because each region of the receptive field overlaps both light and dark stripes.

Opis przestrzennych pól recepcyjnych

- Przestrzenne pola recepcyjne przybliża się często funkcjami Gabora lub ich pochodnymi

$$D_{\mathrm{s}}(x, y) = \frac{1}{2\pi\sigma_x\sigma_y} \exp\left(-\frac{x^2}{2\sigma_x^2} - \frac{y^2}{2\sigma_y^2}\right) \cos(kx - \phi)$$

- Parametry tych funkcji określają własności pola: σ_x i σ_y określają rozmiar pola w kierunkach *x* i *y*, *k* jest preferowaną częstością przestrzenną, a *φ* preferowaną fazą przestrzenną bodźca.

Przestrzenne pola recepcyjne

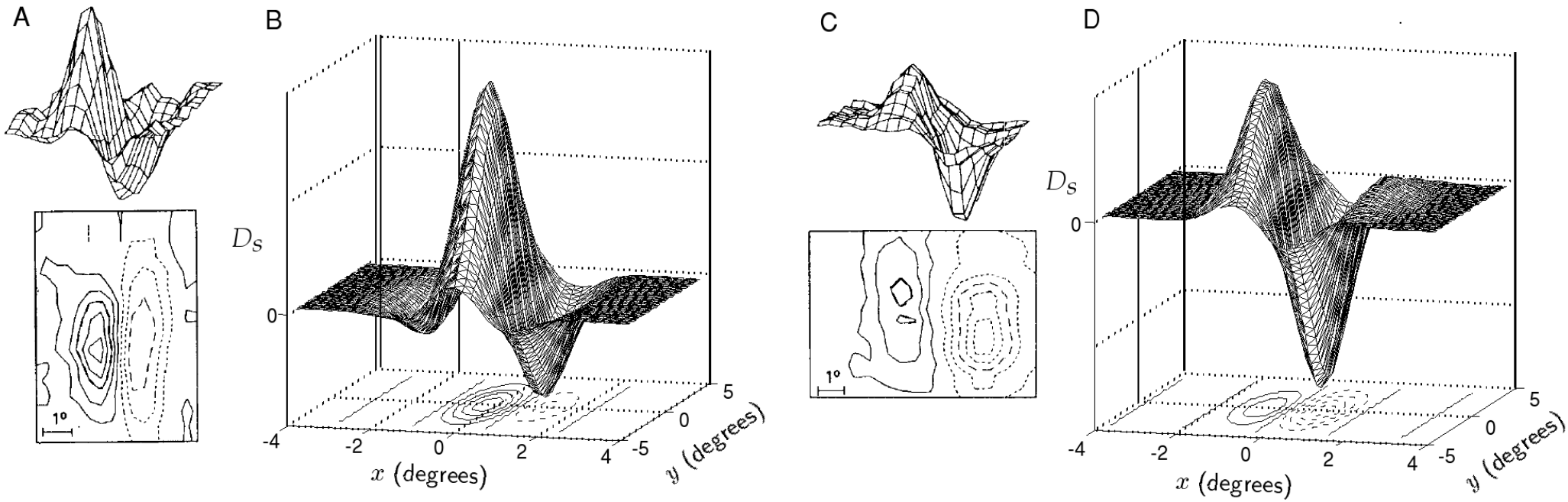

Figure 2.10 Spatial receptive field structure of simple cells. (A) and (C) Spatial structure of the receptive fields of two neurons in cat primary visual cortex determined by averaging stimuli between 50 ms and 100 ms prior to an action potential. The upper plots are three-dimensional representations, with the horizontal dimensions acting as the x-y plane and the vertical dimension indicating the magnitude and sign of $D_s(x, y)$. The lower contour plots represent the x-y plane. Regions with solid contour curves are ON areas where $D_s(x, y) > 0$, and regions with dashed contours are OFF areas where $D_s(x, y) < 0$. (B) and (D) Gabor functions (equation 2.27) with $\sigma_x = 1°$, $\sigma_y = 2°$, $1/k = 0.56°$, and $\phi = 1 - \pi/2$ (B) or $\phi = 1 - \pi$ (D), chosen to match the receptive fields in A and C. (A and C adapted from Jones and Palmer, 1987a.)

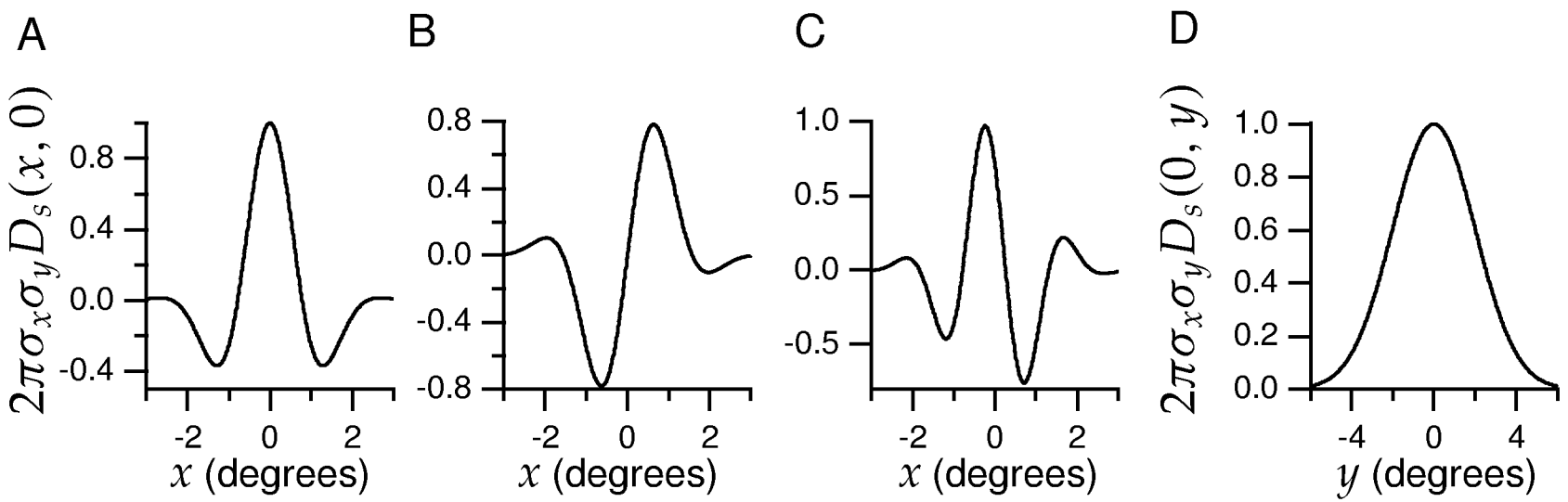

Figure 2.12 Gabor functions of the form given by equation 2.27. For convenience we plot the dimensionless function $2\pi\sigma_x\sigma_y D_s$. (A) A Gabor function with $\sigma_x = 1°$, $1/k = 0.5°$, and $\phi = 0$ plotted as a function of x for $y = 0$. This function is symmetric about $x = 0$. (B) A Gabor function with $\sigma_x = 1°$, $1/k = 0.5°$, and $\phi = \pi/2$ plotted as a function of x for $y = 0$. This function is antisymmetric about $x = 0$ and corresponds to using a sine instead of a cosine function in equation 2.27. (C) A Gabor function with $\sigma_x = 1°$, $1/k = 0.33°$, and $\phi = \pi/4$ plotted as a function of x for $y = 0$. This function has no particular symmetry properties with respect to $x = 0$. (D) The Gabor function of equation 2.27 with $\sigma_y = 2°$ plotted as a function of y for $x = 0$. This function is simply a Gaussian.

Zmiana w czasie przestrzennego pola recepcyjnego

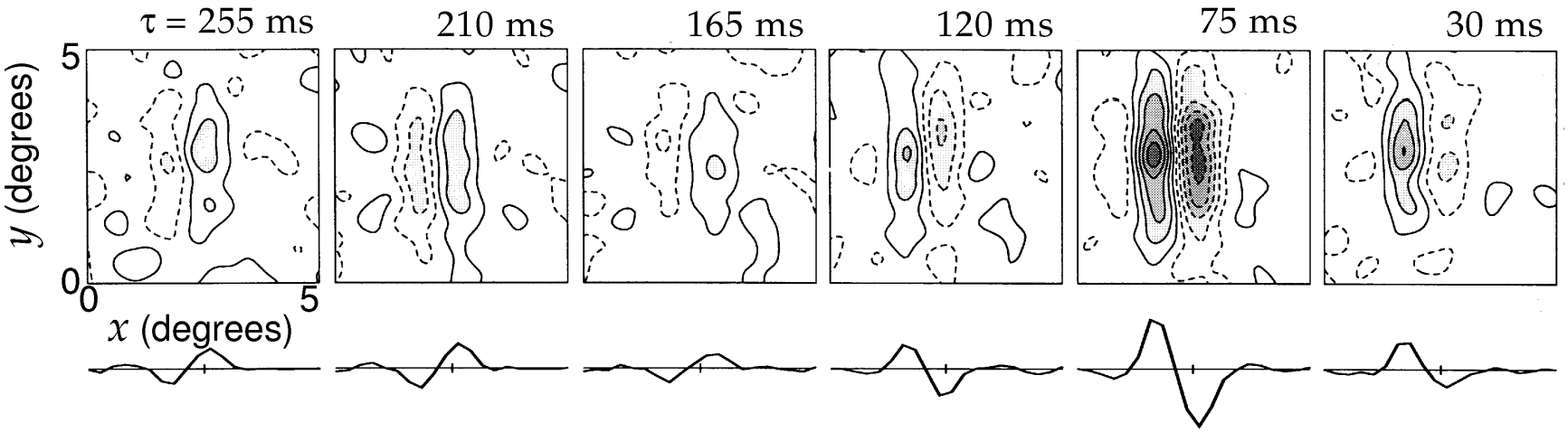

Figure 2.13 Temporal evolution of a spatial receptive field. Each panel is a plot of $D(x, y, \tau)$ for a different value of τ. As in figure 2.10, regions with solid contour curves are areas where $D(x, y, \tau) > 0$ and regions with dashed contours have $D(x, y, \tau) < 0$. The curves below the contour diagrams are one-dimensional plots of the receptive field as a function of x alone. The receptive field is maximally different from 0 for $\tau = 75$ ms with the spatial receptive field reversed from what it was at $\tau = 210$ ms. (Adapted from DeAngelis et al., 1995.)

Czasowe pola recepcyjne

$$D_t(\tau) = \alpha \exp(-\alpha\tau)\left(\frac{(\alpha\tau)^5}{5!} - \frac{(\alpha\tau)^7}{7!}\right)$$

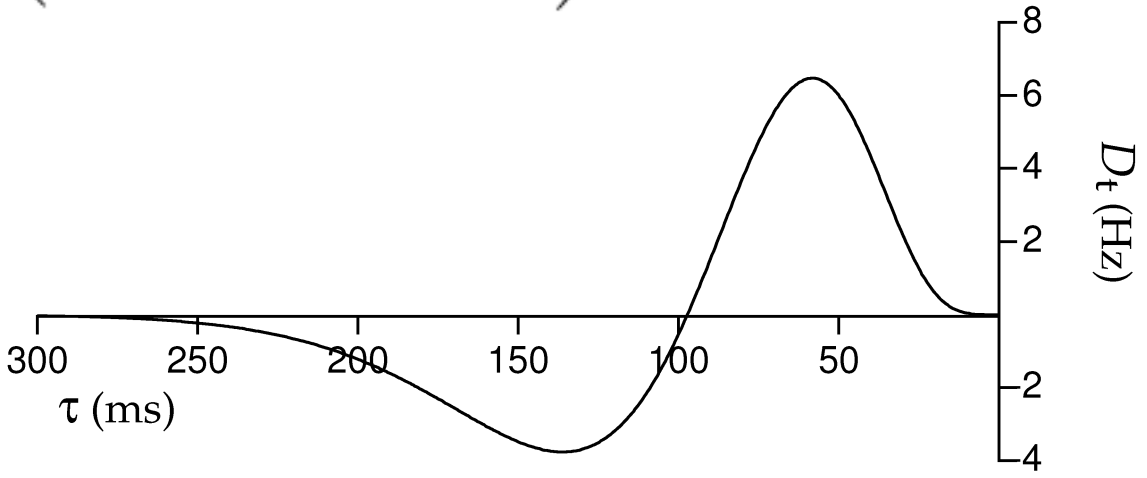

Figure 2.14 Temporal structure of a receptive field. The function $D_t(\tau)$ of equation 2.29 with $\alpha = 1/(15\text{ ms})$.

Zbadamy liniowy człon odpowiedzi na bodziec typu grating

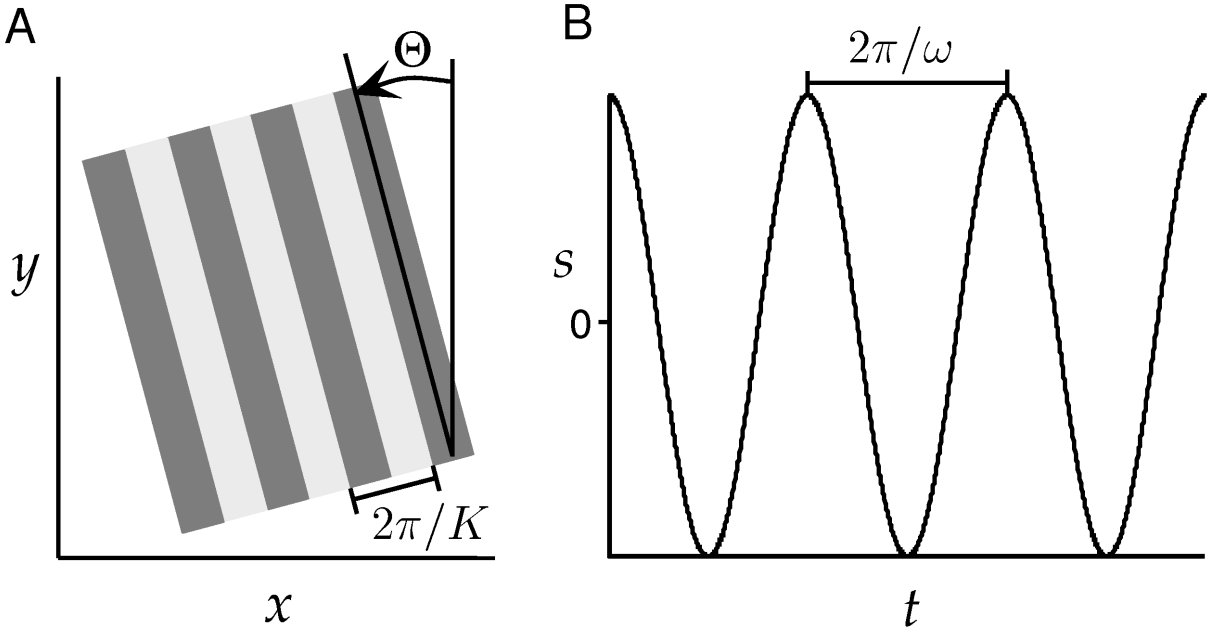

$$s(x, y, t) = A\cos\left(Kx\cos\Theta + Ky\sin\Theta - \Phi\right)\cos(\omega t)$$

Figure 2.8 A counterphase grating. (A) A portion of a square-wave grating analogous to the sinusoidal grating of equation 2.18. The lighter stripes are regions where $s > 0$, and $s < 0$ within the darker stripes. K determines the wavelength of the grating and Θ, its orientation. Changing its spatial phase, Φ, shifts the entire light-dark pattern in the direction perpendicular to the stripes. (B) The light-dark intensity at any point of the spatial grating oscillates sinusoidally in time with period $2\pi/\omega$.

Odpowiedź komórki prostej na bodziec typu grating

- Zbadamy liniowy człon odpowiedzi $L(t) = L_s L_t(t)$

$$L_s = \int dx dy\, D_s(x, y) A \cos\left(Kx\cos(\Theta) + Ky\sin(\Theta) - \Phi\right)$$

$$D_s(x, y) = \frac{1}{2\pi\sigma_x\sigma_y} \exp\left(-\frac{x^2}{2\sigma_x^2} - \frac{y^2}{2\sigma_y^2}\right) \cos(kx - \phi)$$

$$s(x, y, t) = A\cos\left(Kx\cos\Theta + Ky\sin\Theta - \Phi\right)\cos(\omega t)$$

$$\begin{aligned} L_s &= \frac{A}{2}\exp\left(-\frac{\sigma^2(k^2+K^2)}{2}\right)\left(\cos(\phi-\Phi)\exp\left(\sigma^2 kK\cos(\Theta)\right)\right. \\ &\quad \left. + \cos(\phi+\Phi)\exp\left(-\sigma^2 kK\cos(\Theta)\right)\right) . \end{aligned}$$

Odpowiedź komórki prostej na bodziec typu grating

- Jeżeli przestrzenna faza bodźca i preferowana faza pola recepcyjnego wynoszą 0, to

$$L_s = A \exp\left(-\frac{\sigma^2(k^2+K^2)}{2}\right) \cosh\left(\sigma^2 kK \cos(\Theta)\right)$$

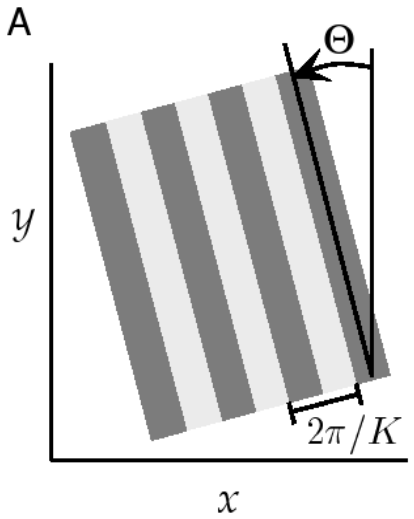

- Jeżeli orientacja bodźca wynosi 0, a preferowana częstość przestrzenna pola k jest niezbyt mała, to

$$L_s = \frac{A}{2} \exp\left(-\frac{\sigma^2(k-K)^2}{2}\right) \cos(\phi - \Phi)$$

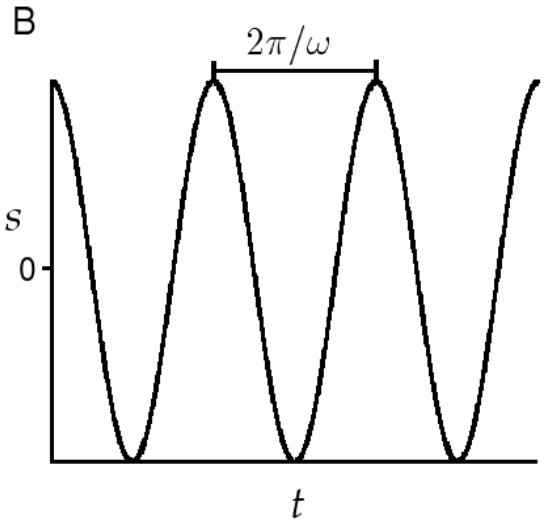

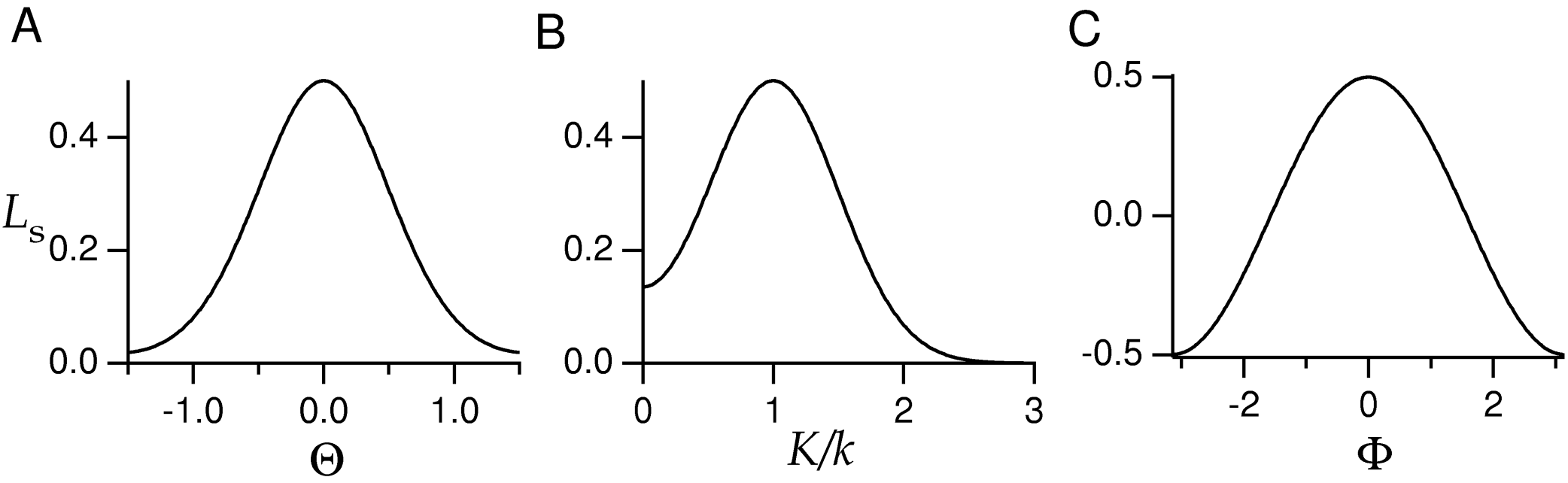

Figure 2.15 Selectivity of a Gabor filter with $\theta = \phi = 0$, $\sigma_x = \sigma_y = \sigma$, and $k\sigma = 2$ acting on a cosine grating with $A = 1$. (A) L_s as a function of stimulus orientation Θ for a grating with the preferred spatial frequency and phase, $K = k$ and $\Phi = 0$. (B) L_s as a function of the ratio of the stimulus spatial frequency to its preferred value, K/k, for a grating oriented in the preferred direction $\Theta = 0$ and with the preferred phase $\Phi = 0$. (C) L_s as a function of stimulus spatial phase Φ for a grating with the preferred spatial frequency and orientation, $K = k$ and $\Theta = 0$.

Szerokość pasma

the Gaussian envelope. The number of subregions within the receptive field is determined by the product $k\sigma_x$ and is typically expressed in terms of a quantity known as the bandwidth b. The bandwidth is defined as $b = \log_2(K_+/K_-)$, where $K_+ > k$ and $K_- < k$ are the spatial frequencies of gratings that produce one-half the response amplitude of a grating with $K = k$. High bandwidths correspond to low values of $k\sigma_x$, meaning that the receptive field has few subregions and poor spatial frequency selectivity. Neurons with more subfields are more selective to spatial frequency, and they have smaller bandwidths and larger values of $k\sigma_x$.

The bandwidth is the width of the spatial frequency tuning curve measured in octaves. The spatial frequency tuning curve as a function of K for a Gabor receptive field with preferred spatial frequency k and receptive field width σ_x is proportional to $\exp(-\sigma_x^2(k-K)^2/2)$ (see equation 2.34 below). The values of K_+ and K_- needed to compute the bandwidth are thus determined by the condition $\exp(-\sigma_x^2(k-K_\pm)^2/2) = 1/2$. Solving this equation gives $K_\pm = k \pm (2\ln(2))^{1/2}/\sigma_x$, from which we obtain

$$b = \log_2\left(\frac{k\sigma_x + \sqrt{2\ln(2)}}{k\sigma_x - \sqrt{2\ln(2)}}\right) \quad \text{or} \quad k\sigma_x = \sqrt{2\ln(2)}\,\frac{2^b+1}{2^b-1}. \tag{2.28}$$

Bandwidth is defined only if $k\sigma_x > (2\ln(2))^{1/2}$, but this is usually the case. Bandwidths typically range from about 0.5 to 2.5, corresponding to $k\sigma_x$ between 1.7 and 6.9.

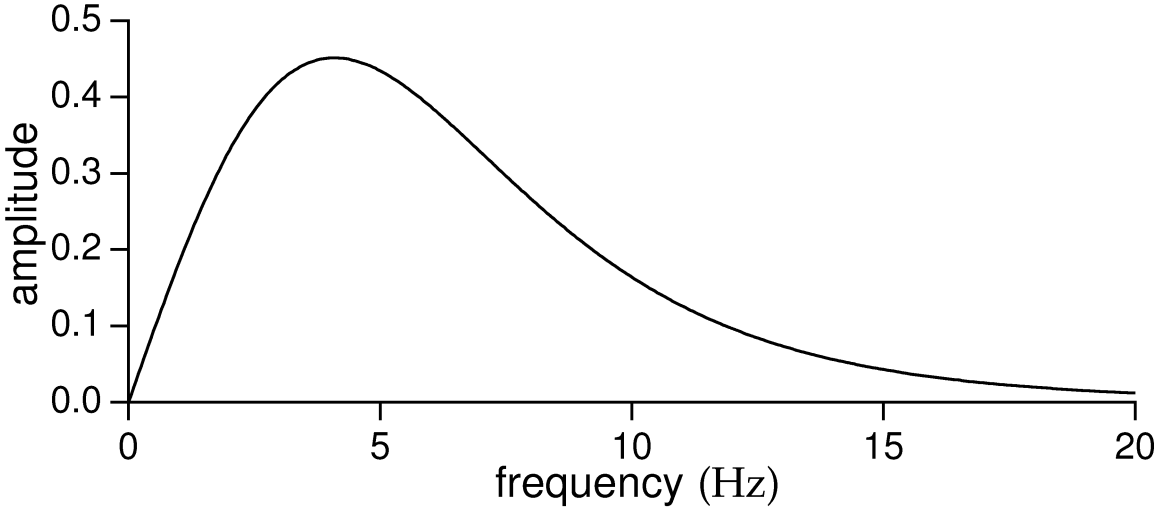

$$L_t(t) = \int_0^\infty d\tau \, D_t(\tau) \cos\left(\omega(t-\tau)\right)$$

Figure 2.16 Frequency response of a model simple cell based on the temporal kernel of equation 2.29. The amplitude of the sinusoidal oscillations of $L_t(t)$ produced by a counterphase grating is plotted as a function of the temporal oscillation frequency, $\omega/2\pi$.

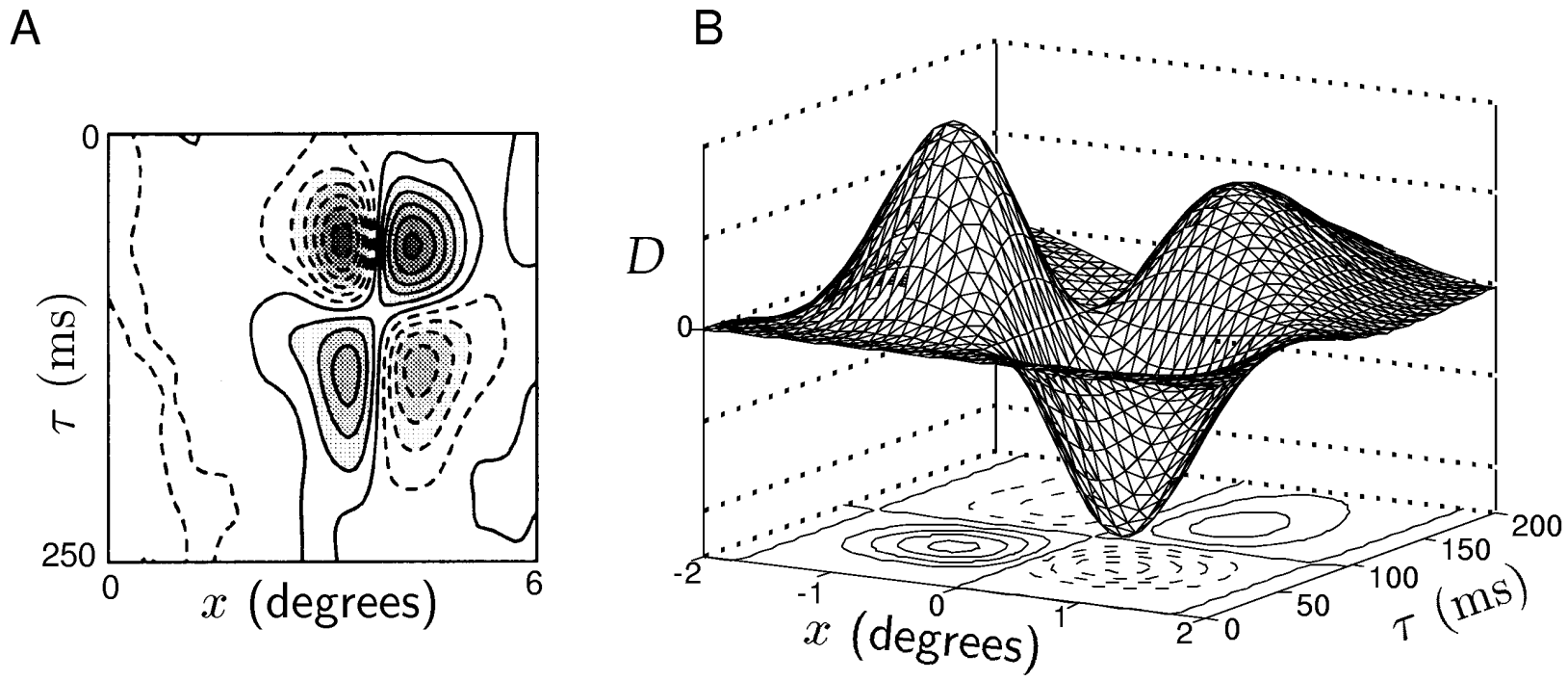

Figure 2.17 A separable space-time receptive field. (A) An x-τ plot of an approximately separable space-time receptive field from cat primary visual cortex. OFF regions are shown with dashed contour lines and ON regions with solid contour lines. The receptive field has side-by-side OFF and ON regions that reverse as a function of τ. (B) Mathematical description of the space-time receptive field in A constructed by multiplying a Gabor function (evaluated at $y = 0$) with $\sigma_x = 1°$, $1/k = 0.56°$, and $\phi = \pi/2$ by the temporal kernel of equation 2.29 with $1/\alpha = 15$ ms. (A adapted from DeAngelis et al., 1995.)

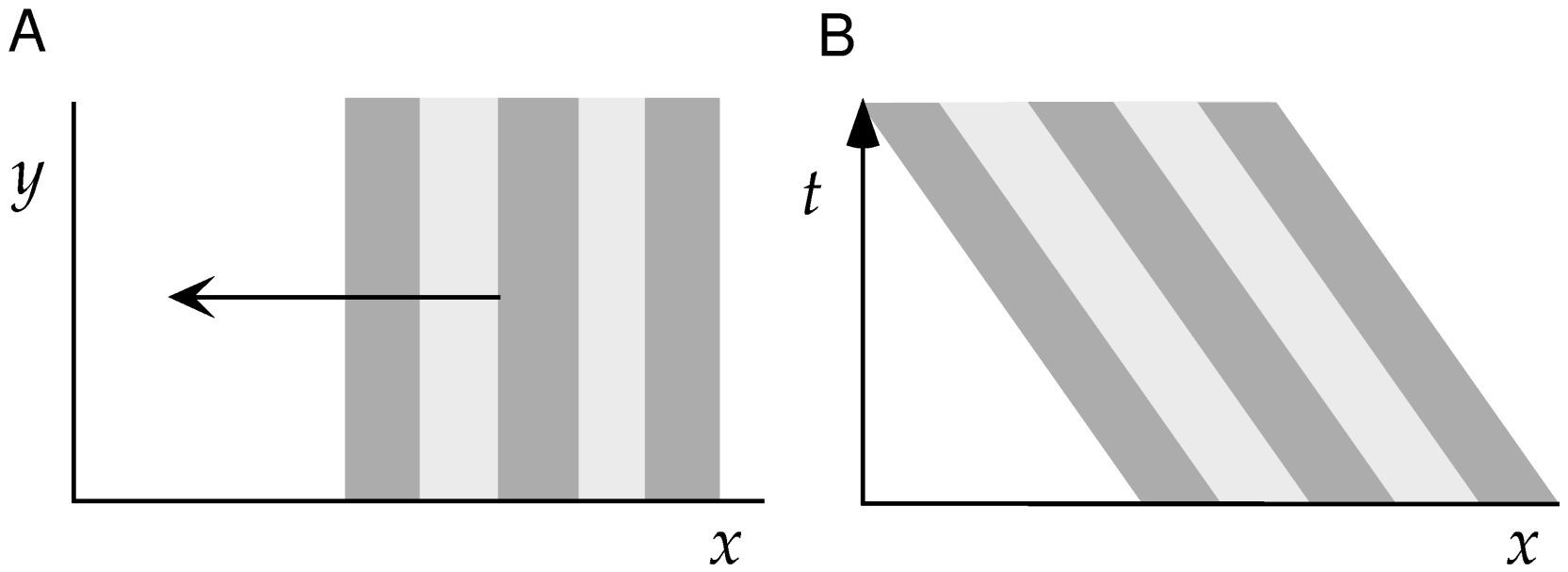

Figure 2.18 Space and space-time diagrams of a moving grating. (A) A vertically oriented grating moves to the left on a two-dimensional screen. (B) The space-time diagram of the image in A. The *x* location of the dark and light bands moves to the left as time progresses upward, representing the motion of the grating.

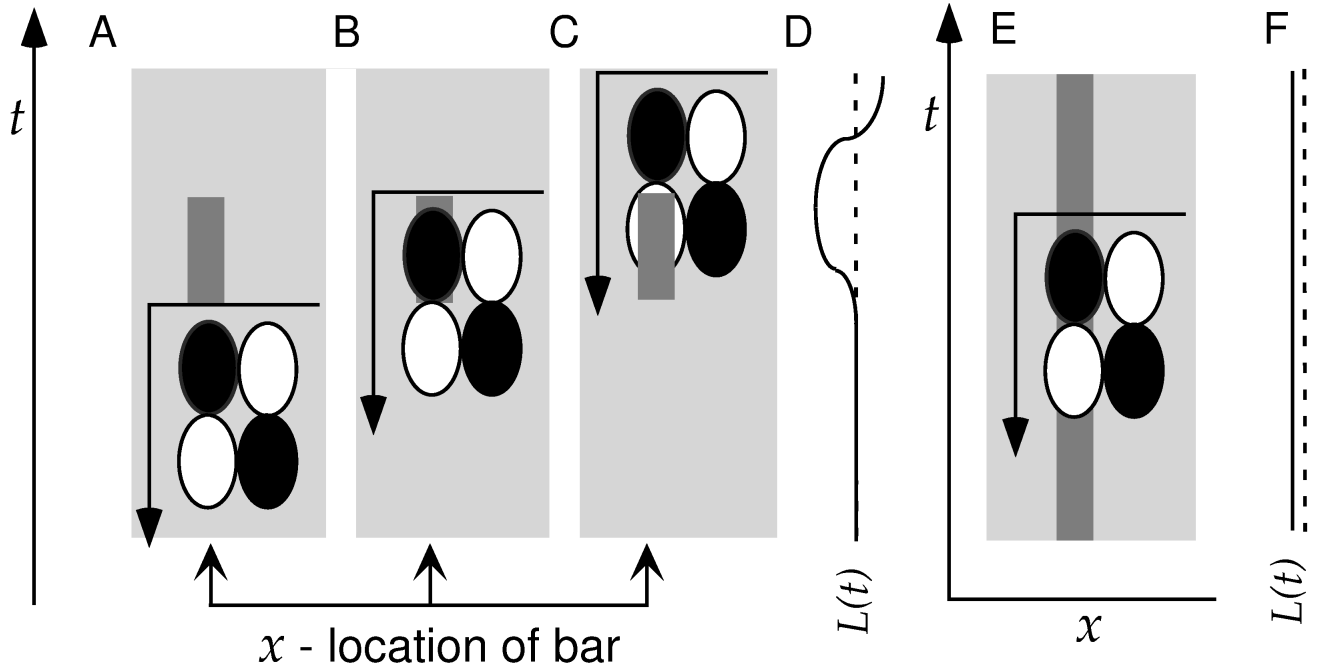

Figure 2.19 Responses to dark bars estimated from a separable space-time receptive field. Dark ovals in the receptive field diagrams are OFF regions and light circles are ON regions. The linear estimate of the response at any time is determined by positioning the receptive field diagram so that its horizontal axis matches the time of response estimation and noting how the OFF and ON regions overlap with the image. (A-C) The image is a dark bar that is flashed on for a short interval of time. There is no response (A) until the dark image overlaps the OFF region (B) when $L(t) > 0$. The response is later suppressed when the dark bar overlaps the ON region (C) and $L(t) < 0$. (D) A plot of $L(t)$ versus time corresponding to the responses generated in A-C. Time runs vertically in this plot, and $L(t)$ is plotted horizontally with the dashed line indicating the zero axis and positive values plotted to the left. (E) The image is a static dark bar. The bar overlaps both an OFF and an ON region, generating opposing positive and negative contributions to $L(t)$. (F) The weak response corresponding to E, plotted as in D.

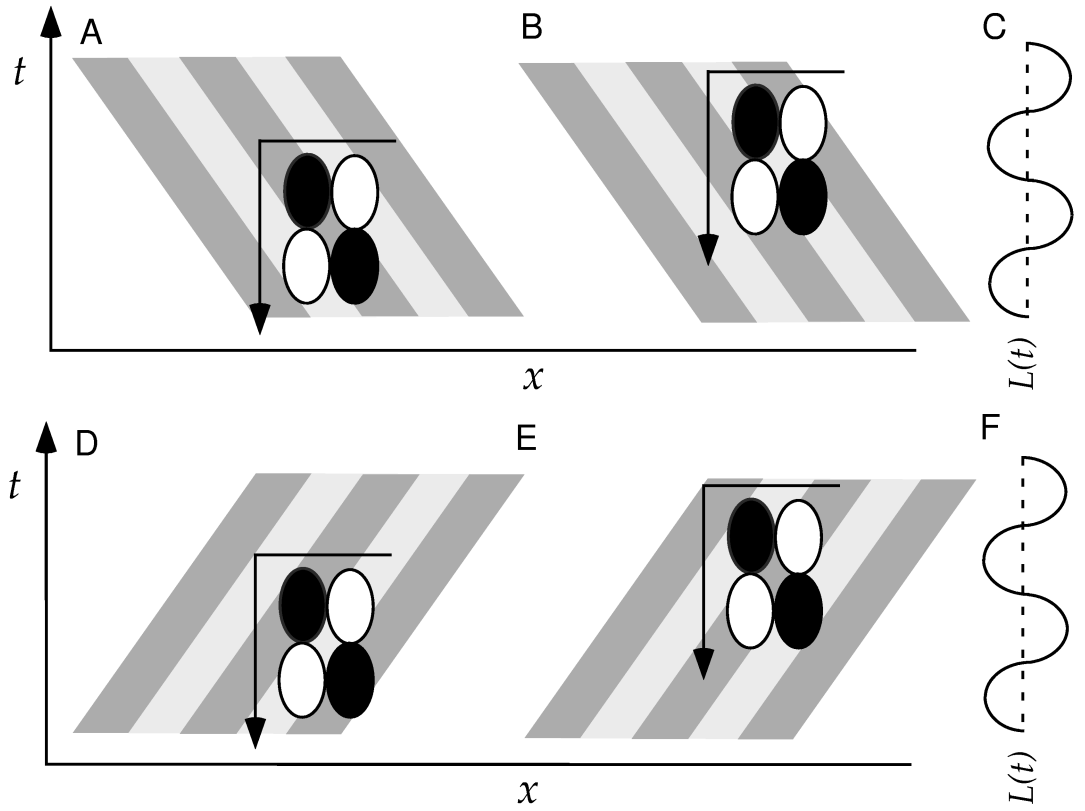

Figure 2.20 Responses to moving gratings estimated from a separable space-time receptive field. The receptive field is the same as in figure 2.19. (A-C) The stimulus is a grating moving to the left. At the time corresponding to A, OFF regions overlap with dark bands and ON regions with light bands, generating a strong response. At the time of the estimate in B, the alignment is reversed, and $L(t)$ is negative. (C) A plot of $L(t)$ versus time corresponding to the responses generated in A-B. Time runs vertically in this plot and $L(t)$ is plotted horizontally, with the dashed line indicating the zero axis and positive values plotted to the left. (D-F) The stimulus is a grating moving to the right. The responses are identical to those in A-C.

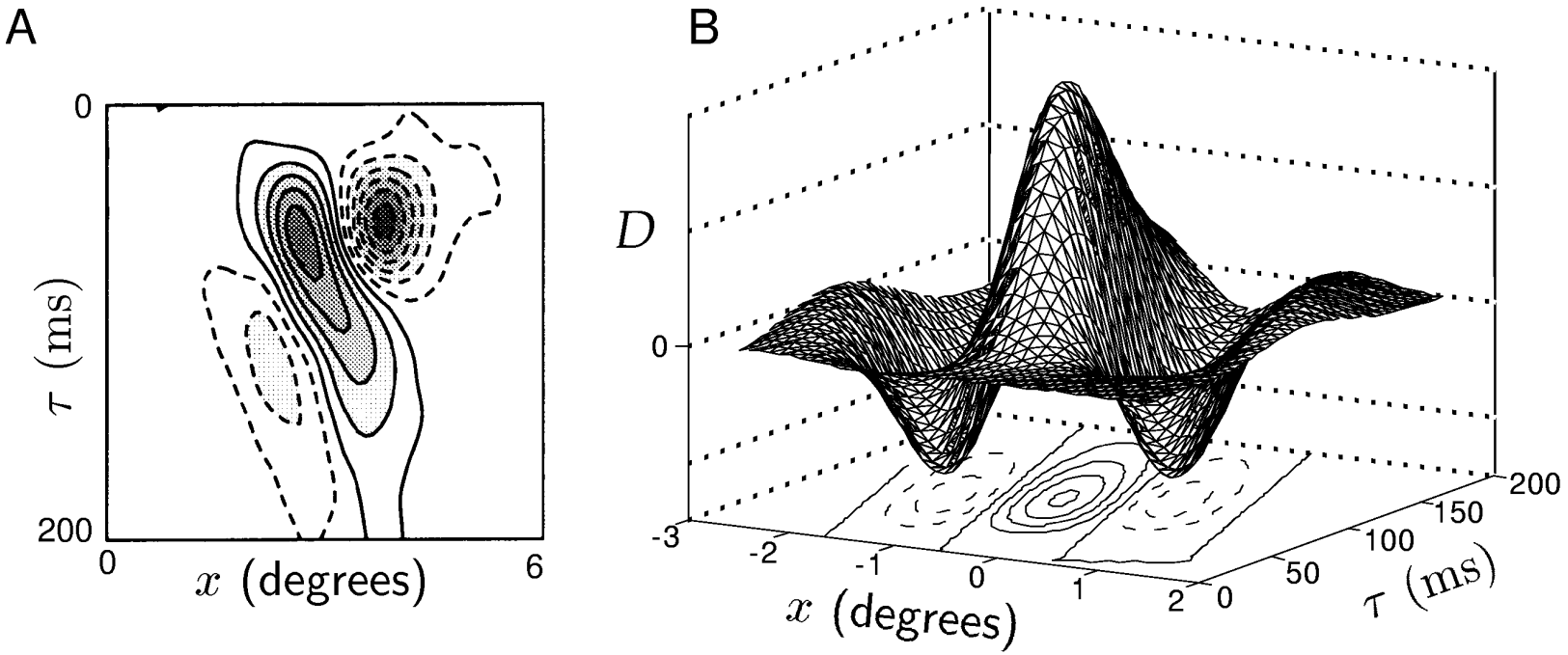

Figure 2.21 A nonseparable space-time receptive field. (A) An x-τ plot of the space-time receptive field of a neuron from cat primary visual cortex. OFF regions are shown with dashed contour lines and ON regions with solid contour lines. The receptive field has a central ON region and two flanking OFF regions that shift to the left over time. (B) Mathematical description of the space-time receptive field in A constructed from equations 2.35 - 2.37. The Gabor function used (evaluated at $y = 0$) had $\sigma_x = 1°$, $1/k = 0.5°$, and $\phi = 0$. D_t is given by the expression in equation 2.29 with $\alpha = 20$ ms, except that the second term, with the seventh power function, was omitted because the receptive field does not reverse sign in this example. The x-τ rotation angle used was $\psi = \pi/9$, and the conversion factor was $c = 0.02\,°/\text{ms}$. (A adapted from DeAngelis et al., 1995.)

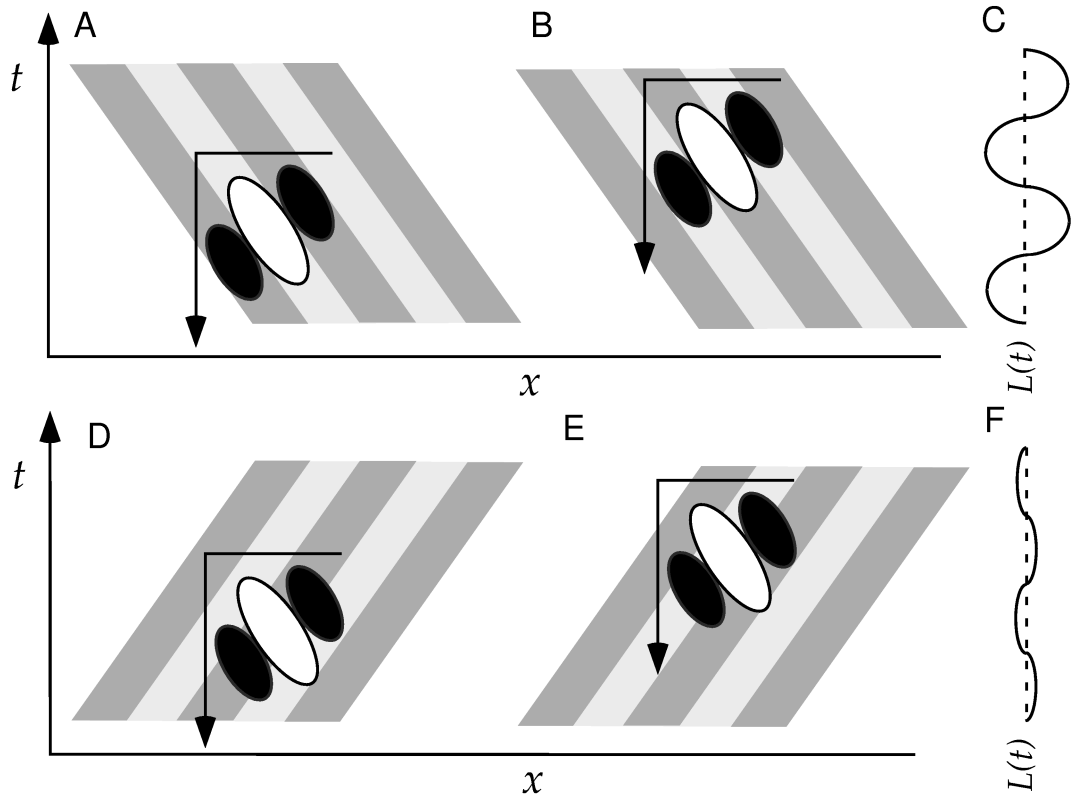

Figure 2.22 Responses to moving gratings estimated from a nonseparable space-time receptive field. Dark areas in the receptive field diagrams represent OFF regions and light areas, ON regions. (A-C) The stimulus is a grating moving to the left. At the time corresponding to A, OFF regions overlap with dark bands and the ON region overlaps a light band, generating a strong response. At the time of the estimate in B, the alignment is reversed, and $L(t)$ is negative. (C) A plot of $L(t)$ versus time corresponding to the responses generated in A and B. Time runs vertically in this plot, and $L(t)$ is plotted horizontally with the dashed line indicating the zero axis. (D-F) The stimulus is a grating moving to the right. Because of the tilt of the space-time receptive field, the alignment with the right-moving grating is never optimal and the response is weak (F).

Komórki złożone

- Komórki proste możemy charakteryzować technikami liniowymi (korelacji odwrotnych)
- Komórki złożone mają cechy, które nie pozwalają na taki prosty opis:
- Obszary takich komórek, które odpowiadają na jasne i ciemne bodźce przekrywają się. Utrudnia to interpretację średnich bodźców wyzwolonych iglicą

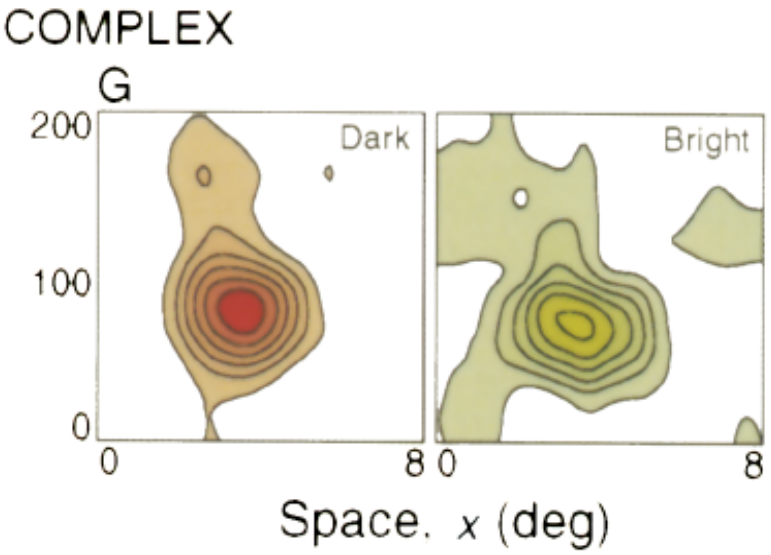

Komórki złożone

- Tym niemniej, komórki złożone również są selektywne na częstość przestrzenną i orientację prążków.
- Inaczej niż komórki proste, komórki złożone odpowiadają na jasne lub ciemne pałeczki bez względu na ich położenie w polu recepcyjnym.
- Podobnie odpowiedzi komórek złożonych na prążki słabo zależą od fazy przestrzennej
- Zatem komórki takie odpowiadają na szczególny typ obrazu niezależnie od jego dokładnego położenia w polu recepcyjnym.

Komórki złożone – charakterystyka czasowa odpowiedzi

- Odpowiedzi komórek złożonych na ruchome prążki są w przybliżeniu stałe, nie oscylują.
- Częstość generacji iglic w odpowiedzi na prążki oscylujące z częstością ω ma składową stałą i składową oscylującą z częstością 2ω (podwojenie częstotliwości).

Metody typu korelacji odwrotnych dla komórek złożonych

- Rozważmy dwie odpowiedzi L_1 i L_2 o preferowanych fazach przestrzennych φ i φ-π/2

$$L_1 = AB(\omega, K)\cos(\phi - \Phi)\cos(\omega t - \delta)$$

$$L_2 = AB(\omega, K)\sin(\phi - \Phi)\cos(\omega t - \delta)$$

- Suma kwadratów nie zależy od φ

$$L_1^2 + L_2^2 = A^2B^2(\omega, K)\cos^2(\omega t - \delta)$$

- Możemy więc opisać niezależną od fazy przestrzennej odpowiedź komórki złożonej

$$r(t) = r_0 + G\left(L_1^2 + L_2^2\right)$$

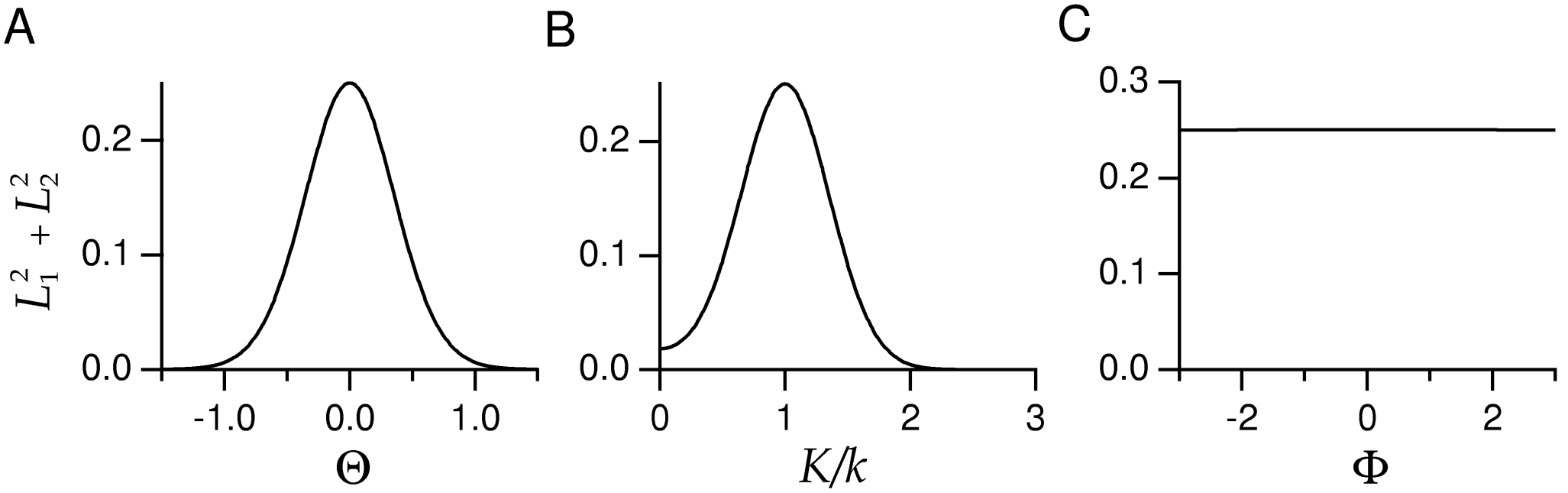

Figure 2.23 Selectivity of a complex cell model in response to a sinusoidal grating. The width and preferred spatial frequency of the Gabor functions underlying the estimated firing rate satisfy $k\sigma = 2$. (A) The complex cell response estimate, $L_1^2 + L_2^2$, as a function of stimulus orientation Θ for a grating with the preferred spatial frequency $K = k$. (B) $L_1^2 + L_2^2$ as a function of the ratio of the stimulus spatial frequency to its preferred value, K/k, for a grating oriented in the preferred direction $\Theta = 0$. (C) $L_1^2 + L_2^2$ as a function of stimulus spatial phase Φ for a grating with the preferred spatial frequency and orientation, $K = k$ and $\Theta = 0$.

Metody typu korelacji odwrotnych dla komórek złożonych

- Tak modelowana odpowiedź

$$L_1^2 + L_2^2 = A^2 B^2(\omega, K) \cos^2(\omega t - \delta)$$

odtwarza efekt podwojenia częstotliwości czasowej, ponieważ

$$\cos^2(\omega t - \delta) = \frac{1}{2}\cos\left(2(\omega t - \delta)\right) + \frac{1}{2}$$

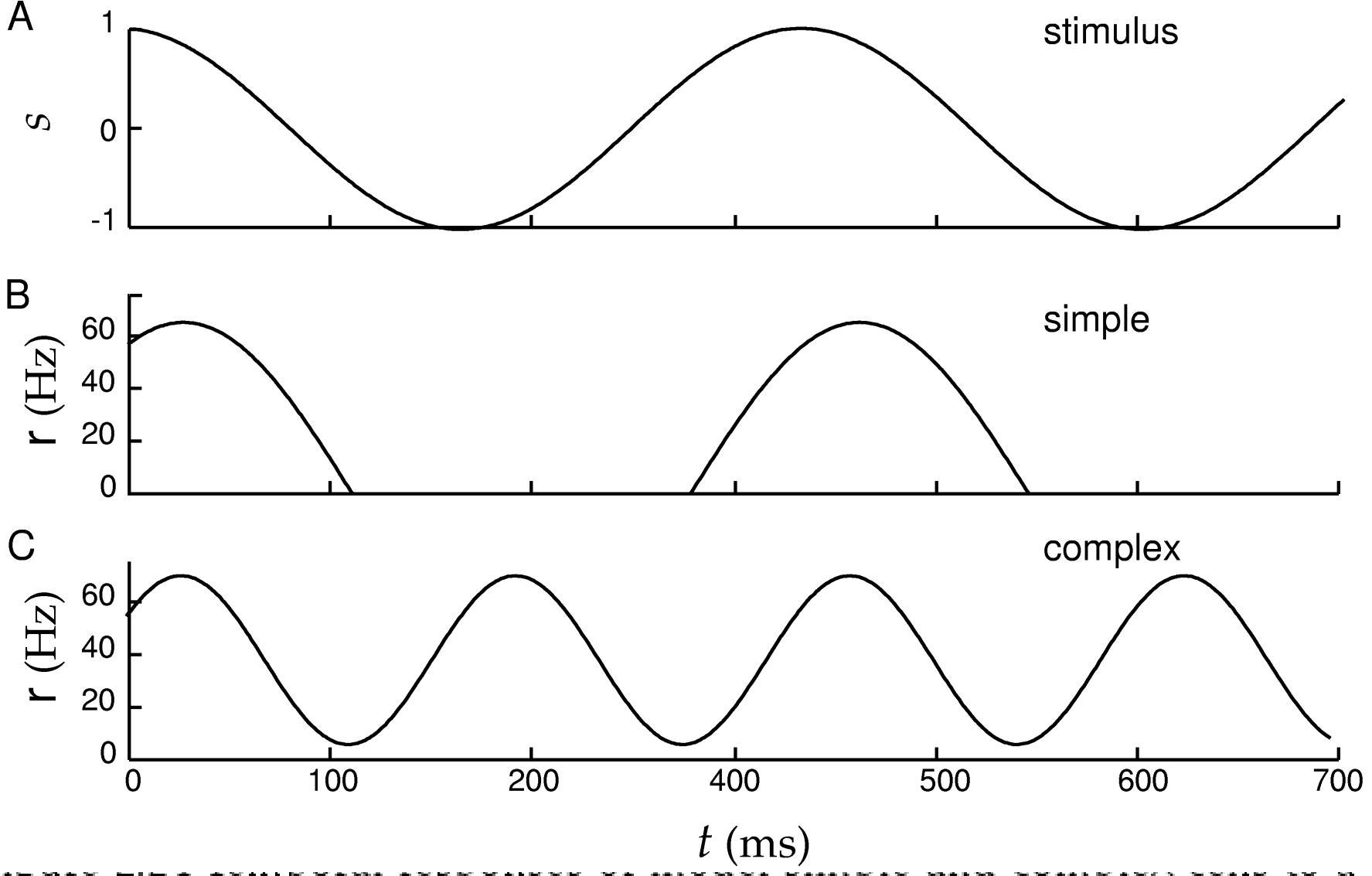

counter-phase grating. (A) The stimulus $s(x, y, t)$ at a given point (x, y) plotted as a function of time. (B) The rectified linear response estimate of a model simple cell to this grating with a temporal kernel given by equation 2.29 with $\alpha = 1/(15\,\text{ms})$. (C) The frequency-doubled response of a model complex cell with the same temporal kernel but with the estimated rate given by a squaring operation rather than rectification. The background firing rate is $r_0 = 5\,\text{Hz}$. Note the temporal phase shift of both B and C relative to A.

Komórki złożone jako kombinacja wejść komórek prostych

- Powyższy model nazywa się “energetyczny”, ponieważ przypomina wzór na energię oscylatora harmonicznego.
- Użyta para filtrów liniowych nazywa się parą kwadraturową (quadrature pair).
- Ze względu na prostowanie połówkowe nie można interpretować tych filtrów jako wejść z komórek prostych.

Komórki złożone jako kombinacja wejść komórek prostych

- Możemy skonstruować ten sam model komórki złożonej biorąc kwadraty odpowiedzi 4 komórek prostych

$$\mathrm{r}(t) = \mathrm{r}_0 + G\left([L_1]_+^2 + [L_2]_+^2 + [L_3]_+^2 + [L_4]_+^2\right)$$

  gdzie różne $[L]_+$ reprezentują odpowiedzi komórek prostych o preferowanych fazach przestrzennych $\phi,\ \phi + \pi/2,\ \phi + \pi,\ \text{and}\ \phi + 3\pi/2$.

- Tej konstrukcji nie należy traktować dosłownie, raczej jako model opisowy.

Pola recepcyjne w siatkówce i LGN

The spatial structure of retinal ganglion and LGN receptive fields is well captured by a difference-of-Gaussians model in which the spatial receptive field is expressed as

$$D_s(x,y) = \pm\left(\frac{1}{2\pi\sigma_{\text{cen}}^2}\exp\left(-\frac{x^2+y^2}{2\sigma_{\text{cen}}^2}\right) - \frac{B}{2\pi\sigma_{\text{sur}}^2}\exp\left(-\frac{x^2+y^2}{2\sigma_{\text{sur}}^2}\right)\right). \tag{2.45}$$

Here the center of the receptive field has been placed at $x = y = 0$. The first Gaussian function in equation 2.45 describes the center, and the second, the surround. The size of the central region is determined by the parameter σ_{cen}, while σ_{sur}, which is greater than σ_{cen}, determines the size of the surround. B controls the balance between center and surround contributions. The $\pm$ sign allows both ON-center (+) and OFF-center (−) cases to be represented. Figure 2.25B shows a spatial receptive field formed from the difference of two Gaussians that approximates the receptive field structure in figure 2.25A.

Pola recepcyjne w siatkówce i LGN

Figure 2.25C shows that the spatial structure of the receptive field reverses over time with, in this case, a central ON region reversing to an OFF region as τ increases. Similarly, the OFF surround region changes to an ON region with increasing τ, although the reversal and the onset are slower for the surround than for the central region. Because of the difference between the time course of the center and of the surround regions, the space-time receptive field is not separable, although the center and surround components are individually separable. The basic features of LGN neuron space-time receptive fields are captured by

$$D(x, y, \tau) = \pm \left(\frac{D_t^{cen}(\tau)}{2\pi\sigma_{cen}^2} \exp\left(-\frac{x^2+y^2}{2\sigma_{cen}^2} \right) - \frac{B D_t^{sur}(\tau)}{2\pi\sigma_{sur}^2} \exp\left(-\frac{x^2+y^2}{2\sigma_{sur}^2} \right) \right) . \quad (2.46)$$

Separate functions of time multiply the center and surround, but they can both be described by the same functions, using two sets of parameters,

$$D_t^{cen,sur}(\tau) = \alpha_{cen,sur}^2 \tau \exp(-\alpha_{cen,sur}\tau) - \beta_{cen,sur}^2 \tau \exp(-\beta_{cen,sur}\tau) . \quad (2.47)$$

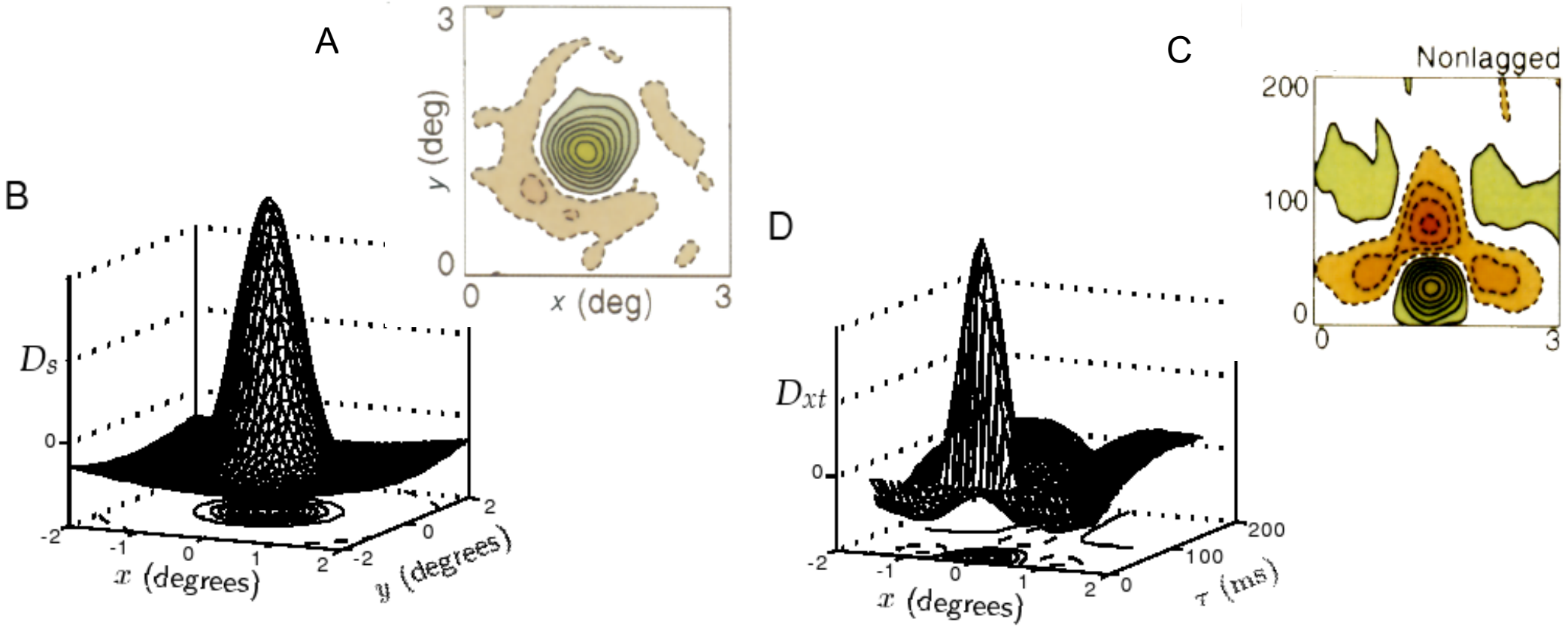

Figure 2.25 Receptive fields of LGN neurons. (A) The center-surround spatial structure of the receptive field of a cat LGN X cell. This has a central ON region (solid contours) and a surrounding OFF region (dashed contours). (B) A fit of the receptive field shown in A using a difference-of-Gaussians function (equation 2.45) with $\sigma_{cen} = 0.3°$, $\sigma_{sur} = 1.5°$, and $B = 5$. (C) The space-time receptive field of a cat LGN X cell. Note that the center and surround regions both reverse sign as a function of τ and that the temporal evolution is slower for the surround than for the center. (D) A fit of the space-time receptive field in C using equation 2.46 with the same parameters for the Gaussian functions as in B, and temporal factors given by equation 2.47 with $1/\alpha_{cen} = 16$ ms for the center, $1/\alpha_{sur} = 32$ ms for the surround, and $1/\beta_{cen} = 1/\beta_{sur} = 64$ ms. (A and C adapted from DeAngelis et al., 1995.)

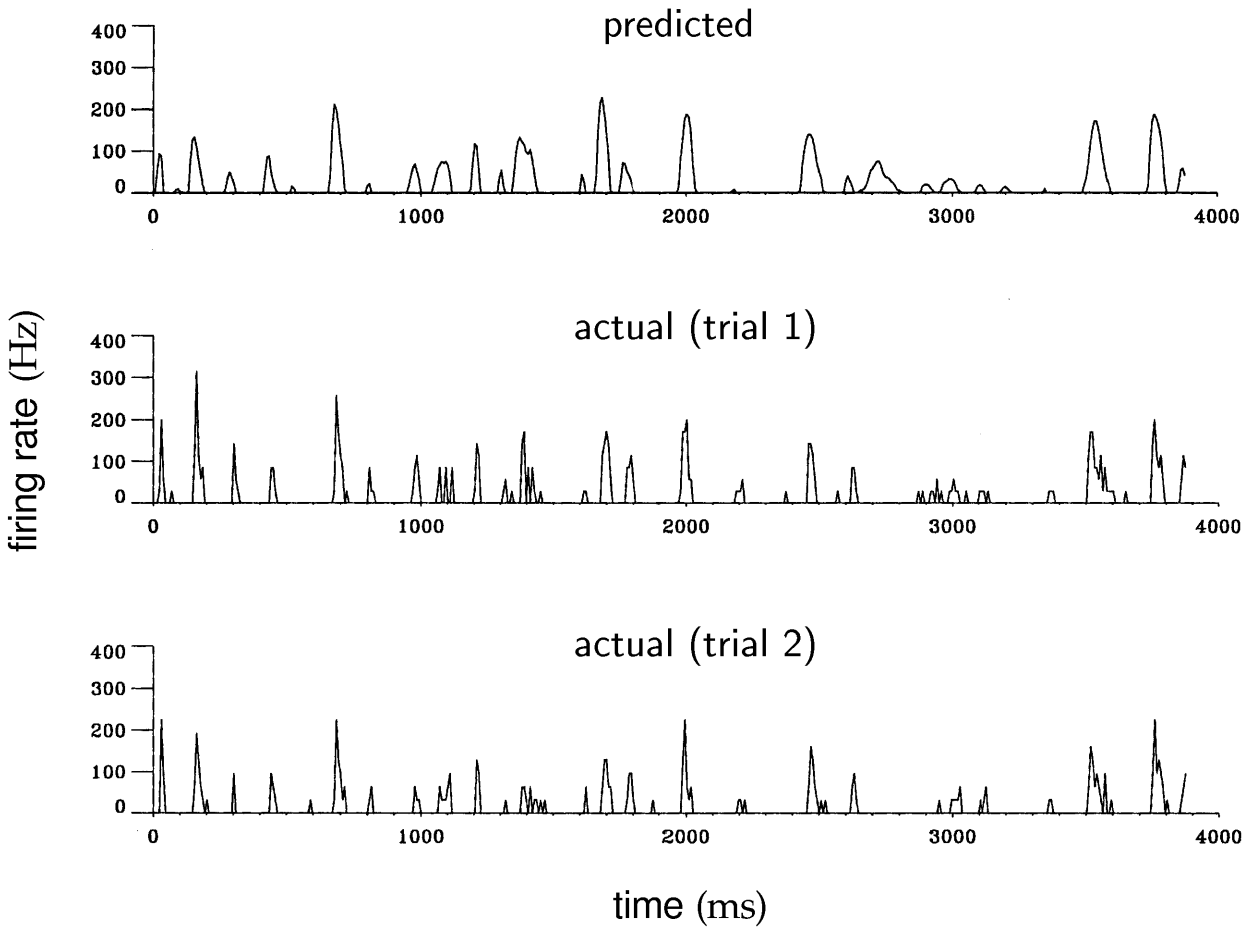

Figure 2.26 Comparison of predicted and measured firing rates for a cat LGN neuron responding to a video movie. The top panel is the rate predicted by integrating the product of the video image intensity and a linear filter obtained for this neuron from a spike-triggered average of a white-noise stimulus. The resulting linear prediction was rectified. The middle and lower panels are measured firing rates extracted from two different sets of trials. (Adapted from Dan et al., 1996.)

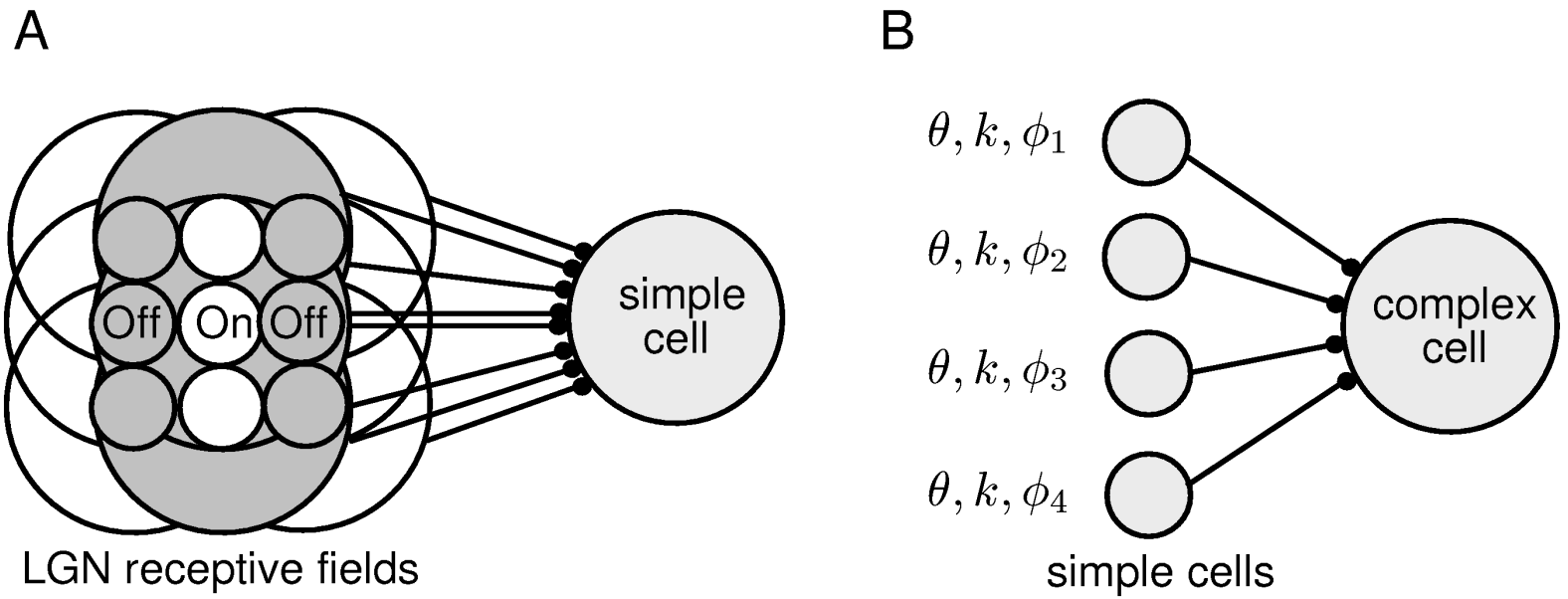

Figure 2.27 (A) The Hubel-Wiesel model of orientation selectivity. The spatial arrangement of the receptive fields of nine LGN neurons are shown, with a row of three ON-center fields flanked on either side by rows of three OFF-center fields. White areas denote ON fields and gray areas, OFF fields. In the model, the converging LGN inputs are summed by the simple cell. This arrangement produces a receptive field oriented in the vertical direction. (B) The Hubel-Wiesel model of a complex cell. Inputs from a number of simple cells with similar orientation and spatial frequency preferences (θ and k), but different spatial phase preferences (ϕ_1, ϕ_2, ϕ_3, and ϕ_4), converge on a complex cell and are summed. This produces a complex cell output that is selective for orientation and spatial frequency, but not for spatial phase. The figure shows four simple cells converging on a complex cell, but additional simple cells can be included to give a more complete coverage of spatial phase.

Receptive-field dynamics in the central visual pathways

Gregory C. DeAngelis, Izumi Ohzawa and Ralph D. Freeman

Trends Neurosci. (1995) 18, 451–458